HELSINKI UNIVERSITY OF TECHNOLOGY
Faculty of Electronics, Communications and Automation
Department of Signal Processing and Acoustics

Renaud-Alexandre Pitaval

Relay Deployment in Single Frequency Network

Master's Thesis submitted in partial fulfillment of the requirements for the degree of Master of Science in Technology.

Espoo (Finland), August 14, 2009

Supervisor: Professor Risto Wichman

Instructor: Taneli Riihonen, M.Sc. (Tech.)

HELSINKI UNIVERSITY OF TECHNOLOGY

ABSTRACT OF THE MASTER'S THESIS

Author:	Renaud-Alexandre Pitaval	
Name of the Thesis:	Relay Deployment in Single Frequency Network	
Date:	August 14, 2009	**Number of pages:** 89
Faculty:	Faculty of Electronics, Communications and Automation	
Department:	Department of Signal Processing and Acoustics	
Supervisor:	Prof. Risto Wichman	
Instructor:	Taneli Riihonen, M.Sc. (Tech.)	

Future wireless communication systems would have to support very high data rates. As this vision is not feasible with the conventional cellular architecture without increasing the density of the base stations, in order to increase the capacity, different transmit diversity schemes have been heavily investigated in the past years. Relaying has been one of those areas investigated and has been proposed as a costly advantageous method to increase the radio coverage area. The scope of this thesis is to build a Matlab simulator for Digital Video Broadcasting - Handheld/Terrestrial (DVB-H/T) and Multimedia Broadcast Multicast Service (MBMS) in 3G systems and evaluate the performance of different relaying concepts. The simulated network is a single-frequency network (SFN) using orthogonal frequency-division multiplexing (OFDM) and the program is a physical layer simulator. The performance metric is the cumulative distribution function of the signal-to-interference-plus-noise-ratio (SINR) for different user positions in the network.

Different simulations have been run to assess the impact of inter-site distance, asynchronity, and other factors such as distance from the border of two SFNs and effect of possible holes in the SFN grid. Then, the focus is on the impact of fixed relaying deployment using the amplify and forward protocol. The impact on the SINR is compared for different relaying gain and densities of relays, as well as different transmission protocol such as the full-duplex and half-duplex protocols. An investigattion is also made of where the relays should be located in the cells to obtain the best performance. Analysis is done at the center of the network and at the border of two SFNs.

Keywords: Radio communication, shadowing cross-correlation, OFDM, relays, gain, duplex, SFN.

Acknowledgements

The research work for this thesis was mostly carried out in the Signal Processing Laboratory at Helsinki University of Technology (TKK) during the years 2007 to 2008 in parallel with my studies as a degree student of the International Master in Communication Engineering.

I wish to express my gratitude to my supervisor, Prof. Risto Wichman, for offering me the opportunity to work with him, his understanding and patience during the writing process, and all the academic helps he provided me.

Many thanks go to my instructor, M.Sc. Taneli Riihonen, for his advices, support and numerous comments.

Among the contributors to this thesis, I thank sincerely William Martin for the language comments.

I would like also to thank my former French professors Jerome Mars and Jocelyn Chanussot, and the international student advisor of ENSIEG Max Ginier-Gillet for all their help, support and kindliness to make possible my stay at TKK possible and even more.

I naturally thank Viet-Anh for all the good working time we have spent together and for other rewarding experiences in the future.

Contents

Abbreviations

3G	3rd Generation
3GPP	3rd Generation Partnership Project
6TU	6 typical urban channel
ADSL	Asymmetric Digital Subscriber Line
A&F	Amplify and forward
AOA	Angle of arrival
AOD	Angle of departure
AP	Access point
AS	Angle spread
AWGN	Additive white Gaussian noise
BPSK	Binary phase shift keying
BS	Base station
CDMA	Code division multiple access
COFDM	Codes orthogonal frequency division multiplexing
CP	Cyclic prefix
CSI	Channel state information
D&F	Decode and forward
DS	Delay spread

DFT	Discrete Fourier transformation
DMT	Discrete multi-tone modulation
DOA	Direction of arrival
DAB	Digital Audio Broadcasting
DVB	Digital Video Broadcasting
DVB-H	Digital Video Broadcasting - Handheld
DVB-T	Digital Video Broadcasting - Terrestrial
FCC	Federal Communications Commission
FF	Fast fading
FFT	Fast Fourier transform
FRS	Fixed relay station
GSM	Global System for Mobile Communication
IEEE	Institute of Electrical and Electronics Engineers
ISD	Inter-site distance
ISDB	Integrated Services Digital Broadcasting
ISI	Inter-symbol interference
ISI	Inter-carrier interference
LAN	Local area network
LOS	Line-of-sight
LTE	Long Term Evolution
LSP	Large scale parameters
MAN	Metropolitan area network
MBMS	Multimedia Broadcast Multicast Service
MIMO	Multiple-input multiple-output

MMAC	Mobile Multimedia Access Communication
MRS	Mobile relay station
MS	Mobile station
NLOS	Non-line-of-sight
NRS	Nomadic relay station
OFDM	Orthogonal frequency division multiplexing
PHY	Physical
PL	Path loss
QAM	Quadrature amplitude modulation
QoS	Quality of service
QPSK	Quadrature phase-shift keying
RMS	Root mean square
RS	Relay station
SF	Shadow fading
SFN	Single frequency network
SINR	Signal to interference and noise ratio
SNR	Signal to noise ratio
TOR	Time of reference
UMTS	Universal Mobile Telecommunications System
WiMAX	Worldwide Interoperability for Microwave Access
WLAN	Wireless local area network
WMAN	Wireless Metropolitan area network

List of Figures

List of Tables

Chapter 1

Introduction

1.1 Background

Future wireless communication network would have to support very high data rates. As this vision is not feasible with the conventional cellular architecture, in order to increase the capacity, different transmit diversity schemes have been investigated heavily in the past years. Relaying has been proposed as a cost effective method to increase both transmission rate and radio coverage area. The main idea of relaying is to support wireless nodes by receiving and retransmitting the signals in addition to the direct communication between a source node and a destination node.

Modern broadcast networks such as Terrestrial Digital Video Broadcasting (DVB-T) make use of wireless networks where multiple transmitters simultaneously transmit the same data. Such wireless networks are termed as single frequency networks (SFN) and are extensively being used throughout Europe.

Orthogonal frequency division multiplexing (OFDM) has been chosen as a multicarrier modulation technology for various high data rate wireless communication systems (e.g. WiMAX, IEEE 802.16, WLAN, IEEE 802.11). OFDM system has also been chosen as the multiplexing technique for the next generation cellular mobile phone networks in the Long Term Evolution (LTE) 3GPP project. In OFDM, the system bandwidth is divided into several orthogonal subchannels. A separate subcarrier is set for each of these narrowband subchannels. Since the OFDM subchannels are designed narrower than the coherence bandwidth of the radio channel, each of these orthogonal subchannels can be treated as a flat fading channel. In addition to this, OFDM is resistant against multipath fading due to utilization of a cyclic prefix, and as a result, OFDM systems are effective against inter-symbol

interference (ISI) in various environments. OFDM modulation is the preferred solution in broadband wireless systems due to its simple equalization and its inherent resistance to interference in multipath propagation environments.

In broadcast networks, the simultaneous transmission of the same data from multiple transmitters causes the effective channel to have a longer delay spread. The existence of a channel delay spread longer than the cyclic prefix length causes severe performance degradation due to the contribution of inter-symbol interference and inter-carrier interference (ICI) into the received OFDM symbol. The introduction of relays in the network, while increasing the received signal strength, will extend further the delay spread of the effective channel and as a consequence increase the interference.

1.2 Research problem and scope

The objective of this thesis is to study the impact of a fixed relay deployment in a single frequency network using OFDM. A Matlab simulator has been built for an OFDM-based SFN and the performance of different relaying concepts has been evaluated in downlink broadcast communication. We have observed and analyzed the evolution of the signal-to-interference-plus-noise-ratio (SINR) distribution for different changes of the SFN parameters, relay densities, topologies and protocols. We have studied if the network can be established efficiently in the sense of maximizing the SINR distribution in a cell.

1.3 Outline of the thesis

The rest of this thesis is organized as follows. The first part of the thesis consists of theoretical works. In the first chapter, the state of the art in wireless communication is reviewed through the radio channel model. Chapter 3 gives a extensive literature review on correlations among the large-scale parameters defined in Chapter 2. The principles of OFDM are introduced in Chapter 4, as well as a performance metric for this kind of system, the average SINR. Chapter 5 reviews some basic relaying concepts and gives theoretical results for the derivation of the average SINR defined in Chapter 4 using relay transmission.

The second part of the thesis presents the simulation works and conclusions. Chapter 6 describes the simulator development. We describe in this chapter the network architecture, the simulation scenario and the chosen parameters. Chapter 7 presents the simulation results for a classical SFN in a first step and then with the

introduction of relays in the network. The impact of the relays gain, transmission protocol, topologies and densities are among the things studied. The analysis is made both at the center of the network and at its border. Finally in the last chapter, we conclude and give an outlook to topics of future research.

Chapter 2

Review of the mobile radio channel

This chapter reviews the classical modeling of wireless mobile communications channels. This type of channel is not only perturbed by additive noise, but also by time-varying multipath propagation. The great variation of the resulting received signal's amplitude, referred to as signal fading, which may vary with time, frequency and geographical position is often modeled as a random process. This chapter is a short summary of the analysis presented in [16, 19, 47, 56].

2.1 Time-varying multipath channel

The propagation environment of the wireless channel is plagued by different physical nuisances, the most important to deal with being multipath propagation and Doppler effect.

2.1.1 Multipath propagation

In a wireless channel, the transmitter and the receiver are surrounded by objects which reflect, diffract and scatter the transmitted signal via different routes with different attenuations, delays and phases. Transmissions are severely degraded by the effects of so-called multipath propagation. Examples of obstructions include buildings, trees, and cars in outdoor settings, and walls, furniture, and people in indoor settings. Scattering and propagation over longer distances increasingly attenuates signal power (path loss effect). Thus, a radio receiver observes multiple attenuated and time-delayed versions of the transmitted signal that are further corrupted by

additive receiver thermal noise and other forms of interference. The copies of the transmitted signal might add constructively, thereby increasing the signal-to-noise ratio (SNR), or destructively, thereby decreasing the SNR. Usually, the effects of path loss and fading are modeled as a time-varying linear filter.

2.1.2 Doppler effect

As a result of the motion of the receiver (or of some scatterers), a change from the Doppler effect occurs in the observed frequency f of waves from different directions. This variation, called the Doppler shift f_d, is proportional to the mobile velocity. For wireless propagation, the speed of the waves through the atmosphere is equal to the speed of light c, then the observer detects waves with a frequency f is given by

$$f = f_c \left(\frac{c}{c \pm v_r} \right) = f_c \left(1 \pm \frac{v_r}{c \pm v_r} \right).$$

where v_r is the speed of the source with respect to the medium, radial to the observer, and f_c is the frequency emitting by the source.

With relatively slow movement, v_r is small in comparison to c and the equation approximates to

$$f \approx f_c \left(1 \pm \frac{v_r}{c} \right).$$

The radial velocity does not remain constant, but instead varies as a function of the angle between its line of sight and the mobile's velocity:

$$v_r = v \cdot \cos\theta$$

where v is the velocity of the receiver with respect to the medium, and θ is the angle of arrival of the wave with respect to the direction of motion of the receiver.
So,

$$f = f_c \left(1 \pm \frac{v \cos\theta}{c} \right) = f_c \pm f_d$$

where $f_d = \frac{v}{c} f_c \cos\theta = \Delta f_d \cdot \cos\theta$ is the Doppler shift, and Δf_d the maximum Doppler shift or Doppler spread which occurs for $\theta = 0$.
Thus the received signal through a multipath channel has a frequency range of $(f_c - \Delta f_d) \leq f \leq (f_c + \Delta f_d)$. With relative motion of the transmitters, receivers, and scatterers in the multipath environment, SNR fluctuations occur across both time and frequency, and are generally called fading.

2.2 Baseband channel model

Signals transmitted over mobile radio channels contain a set of frequencies within a bandwidth which is narrow compared with the central frequency of the channel. In simulations based on a 3GPP parameter (Table 6.4), a 10 MHz signal is modulated onto a carrier at 2GHz, the resulting ratio is 10 MHz/2 GHz = 0.05%. Since the carrier does not carry information, the bandpass transmitted signal $s_c(t)$ is often expressed as a function of the baseband signal $s(t)$, and the channel is model in baseband representation

$$s_c(t) = \mathrm{Re}\left(s(t)e^{j2\pi f_c t}\right).$$

The received bandpass signal is the sum of multiple attenuated and delayed copies of the original signal:

$$r_c(t) = \sum_i a_i(t)s_c(t-\tau_i(t)) = \mathrm{Re}\left(\sum_i a_i s(t-\tau_i(t))e^{j2\pi f_c(t-\tau_i(t))}\right)$$

where $\tau_i(t)$ and $a_i(t)$ are respectively the time varing delay and path gain of the i^{th} path depending on the reflection coefficient and scattering characteristics of the scatterer. Here the noise effects are omitted to lighten the writing.

Equivalently, we can consider the received baseband signal

$$r(t) = \sum_i a_i(t)e^{-j2\pi f_c\tau_i(t)}s(t-\tau_i(t)).$$

Now considering motion at the receiver, the Doppler effect is modeled as follows in the received signal:

$$r(t) = \sum_i a_i(t)e^{j2\pi(\nu_i t - f_c\tau_i(t))}s(t-\tau_i(t)) = \sum_i a_i(t)e^{j\theta_i(t)}s(t-\tau_i(t))$$

where ν_i and θ_i are the Doppler shift and the fading phase of the ith path, respectively. The equation can be modified as follows to obtain a linear filter:

$$r(t) = \sum_i a_i(t)e^{j\theta_i(t)}\int_{-\infty}^{\infty} s(t-\tau)\delta(\tau-\tau_i(t))\mathrm{d}\tau$$

$$r(t) = \int_{-\infty}^{\infty} s(t-\tau)\sum_i a_i(t)e^{j\theta_i(t)}\delta(\tau-\tau_i(t))\mathrm{d}\tau.$$

By setting $h(\tau,t) = \sum_i a_i(t)e^{j\theta_i(t)}\delta(\tau - \tau_i(t))$, which is a time variant linear filter,

$$r(t) = \int_{-\infty}^{\infty} s(t-\tau)h(t,\tau)\mathrm{d}\tau = [s * h(\cdot,t)](t).$$

Thus the time-variant impulse response of the discrete M-path channel is:

$$h(\tau,t) = \sum_{k=0}^{M-1} a_k(t)e^{j2\pi(\nu_k t - f_c\tau_k(t))}\delta(\tau - \tau_k(t)) \quad (2.1)$$

$$h(\tau,t) = \sum_{k=0}^{M-1} a_k(t)e^{j\theta_k(t)}\delta(\tau - \tau_k(t)). \quad (2.2)$$

If the mobile stations move in a small area with a constant speed under one transmission frame, a_i, τ_i, θ_i and the total number of paths are approximately constant. No delay changes in the envelope are mentioned, only the frequency offset of the carrier, due to its relatively small bandwidth as explained at the beginning of this paragraph.

From Equation (2.2), a Fourier transform relative to the time delay domain τ results in the time variant-transfer function, which gives the fading profile as a function of signal frequency and movement time,

$$H(f,t) = \mathcal{F}_\tau\{h(\tau,t)\} = \sum_{k=0}^{M-1} a_k(t)e^{j\theta_k(t)}e^{-j2\pi f\tau_k}. \quad (2.3)$$

As one can see from Equation (2.3), in practice a wireless transmission in a certain environment including a certain velocity of objects is described by two values, the Doppler spread Δf_d and the delay spread $\Delta\tau$, which described respectively the time and frequency selectivity behavior of the channel.

2.2.1 Time selectivity

The Doppler shift induces frequency dispersion. Due to Doppler spreading, the fading would also vary in time. The wireless channel, therefore, becomes time selective. At some time instances the received signal is not attenuated and could appear even enhanced; at other time instances the signal is severely attenuated. Thus the channel model varies in time.

The time selectivity behavior caused by the Doppler spread Δf_d depends on the ratio of the symbol duration T_s and the channel coherence time $T_{coh} \propto \frac{1}{\Delta f_d}$

proportional to the inverse delay spread. For easier characterization, the product $T_s \cdot \Delta f_d$ is taken into consideration.

- If $\Delta f_d \cdot T_s \gg 1$, the fading varies during one symbol duration and the channel is time selective. Channel estimation is not anymore possible, only non-coherent detection and differential modulation can be applied.
- In contrast, if $\Delta f_d \cdot T_s \ll 1$, then the channel is not time selective. Channel estimation is possible, coherent detection and normal modulation can be applied (QPSK, 16-QAM ...).

These two conditions are also sometimes named fast or fastly and slow or slowly fading, respectively, but this notation can be confusing with the statistical notion of small scale and large scale fading described later in this thesis. In a typical wireless system, Doppler spreads may range from 1 to 100 Hz, corresponding to coherence times from 0.01 to 1 s, while symbol duration ranges from $2 \cdot 10^{-4}$ to $2 \cdot 10^{-6}$ second [9]. Thus, blocks with a length ranging from 200 symbols to 10^6 symbols are affected by approximately the same fading. As a consequence, in system models, the fading is often assumed constant during a transmission block and varying from one transmission block to another, this is referred to as *block fading*.

The following will focus only on the impact of delay spread, leading to the characterization of a wideband and narrowband channel.

2.2.2 Frequency selectivity

A channel is said to be a wide or a narrowband one depending on the ratio of the signal bandwidth W and the coherence bandwidth $B_{coh} \propto \frac{1}{\Delta\tau}$ proportional to the inverse delay spread. For easier characterization, the product $W \cdot \Delta\tau$ is usually taken into consideration. Regarding the accuracy given by the sampling rate corresponding to the receiver bandwidth, the multiple received echoes of the transmitted signal are grouped in a cluster of no separable components. If the delay spread is large compared to the sampling time, the received signal will be highly distorted; if not, the multiple echoes will not greatly affect the signal.

Two types of channels are differentiated leading to different models:

- Flat/narrowband/no frequency selective channel: $W \cdot \Delta\tau \ll 1$. Regarding the accuracy given of the receiver bandwidth, there are no separable multipath components, the channel is thus modeled by a single tap channel.
- Widedand/frequency selective channel: $W \cdot \Delta\tau \gg 1$. The signal is seen by the receiver to consist of separable multipath components. The channel is modeled as a multi-tap channel.

The notion of frequency selectivity increases with regard to the frequency dependence of the transfer function. Since the delays τ_k are different for several paths, some frequencies are attenuated while others are not. If the delay difference between the paths is very small or even does not exist, then frequencies are attenuated in the same manner by the delay spread. The delay spread gives the speed of change of the mobile channel in the frequency domain.

Narrowband channel model

In the narrowband channel, multipath fading comes from path length differences between rays coming from different scatterers. Nevertheless, all rays arrive at essentially the same time with regard to the sampling frequency of the receiver, so the fading affects all frequencies in the same way and it can be modeled as a single multiplicative process. Consider a receiver, which moves through a multipath environment with a certain fixed speed. Further consider all path delays in this environment to be negligibly small, such that $s(t - \tau_i) \approx s(t)$. Then the received signal is simplified and turns into

$$r(t) = s(t) \cdot \sum_i a_i(t) e^{j\theta_i(t)} = s(t) \cdot a(t) e^{j\theta(t)} = s(t) \cdot h(t)$$

where $a(t)$ is the complex fading coefficient at time t. Here $h(t)$ is called the complex gain of the channel. In this case, the input and output of the channel are connected by a simple multiplicative relationship.

Wideband channel model

The wideband mobile radio channel has assumed increasing importance in recent years as transmission bandwidths increase to support multimedia services. In practice, the impulse response would always be experienced via a receiver filter of finite bandwidth, which will be unable to distinguish between a discrete and continuous case. Therefore, the effects of scatterers in discrete delay ranges are regrouped into individual taps with the same delay.

The model of N-tap delay channel is as follows:

$$h(\tau, t) = \sum_{n=1}^{N} h_n(t) \delta(\tau - \tau_n)$$

where

$$h_n(t) = \sum_{k=0}^{M_n-1} a_k(t) e^{j\theta_k(t)}.$$

The separable multipath components arrive at different delays; if a too long delay spread occurs, the previous symbol is still arriving at the receiver when the initial energy of the next symbol arrives. The wideband channel can be regarded as a combination of several paths subject to narrowband fading, combined together with appropriate delays. Since large delays involve long paths between the scatterers and the terminals, there is a tendency for the power per tap delay to reduce with increasing delay. The taps are usually assumed to be uncorrelated with each other, since each arises from scatterers which are physically distinct and separated by many wavelengths.

It is often practical to regard the power delay profile of the channel in function of the tapped delay line

$$p(\tau, t) = |h(\tau, t)|^2 = \sum_{n=1}^{N} |h_n(t)|^2 \delta(\tau - \tau_n(t)).$$

This power delay profile is characterized by the delay spread: the maximum delay spread $\Delta\tau$ or root-mean-square (RMS) delay spread $\Delta\tau_{rms}$. If the RMS delays spread is very much less than the symbol duration, no significant interference among the transmitted frames is encountered and the channel may be assumed narrowband.

Here is a summary table:

Selectivity/ fading changes in	Cause	parameter	Effects
time	motion	Δf_d	frequency dispersion
frequency	multipath	$\Delta\tau$	time dispersion

2.3 Statistical channel modeling

In the previous section the time variability of the fading has been addressed, no attempt is usually made to predict the exact value of the signal strength arising from multipath fading, as this would require a very exact knowledge of the position and electromagnetic characteristics of all the scatterers. Instead a statistical description

is used, which will be different for different environments (mainly Line-Of-Sight (LOS) / Non-Line-Of-Sight (NLOS) propagation).

Statistical models are traditionally based on measurements made for a specific system or spectrum allocation. When modeling the channel, the propagation effects are normally broken down into three main categories: path loss (PL), shadow fading (SF), and fast fading (FF). The shadow fading and fast fading are also commonly known as large scale and short scale fading respectively, where the name refers to the size of the area where substantial correlation is observed. The received signal power attenuation in mobile wireless communications can be, so, described as the product of three-scale factors:

- the deterministic part of the local average received power which is distance-dependent (average path loss)
- the stochastic part of the local average received power often modeled as a lognormal variation (large-scale fading also called shadow fading or slow fading)
- and a small-scale fading due to movements in the order of the wavelength (fast fading)

$$ChannelGain = (PathLoss)^{-1} \times ShadowFading \times FastFading.$$

Let us assume flat fading, the instantaneous power of the channel is $P_h = |h|^2$, averaging on the local area one obtain $E_h = \mathcal{E}\{P_h\} = PL^{-1} \times SF$ and now averaging on a large area $\mathcal{E}\{PL^{-1} \times SF\} = PL^{-1}$. Sometimes the fast fading refers to the whole instantaneous variation and not only the variation around the local mean.

Several models have been investigated for path loss. Shadow fading is the least well understood of these three factors. It has been empirically observed to obey approximately lognormal distribution in a wide variety of propagation environments [28,56]. This lognormality is usually explained as a result of multiplication of large number of random attenuating factors in the radio channel while this assumption is difficult to justify from a physical propagation point of view; an interesting discussion with a alternative model may be found in [55]. The fast fading of a radio channel results from multipath propagation due to reflection, diffraction and scattering. These physical phenomena could arise when the transmitted signal encounters obstacles (like buildings, mountains...) in its propagation path. For small-scale fading, numerous statistical models have been proposed, most notably the Rayleigh, Rice and Nagakami-m probability distributions. In order to enhance the design of mobile radio systems, the modeling of fading is essential.

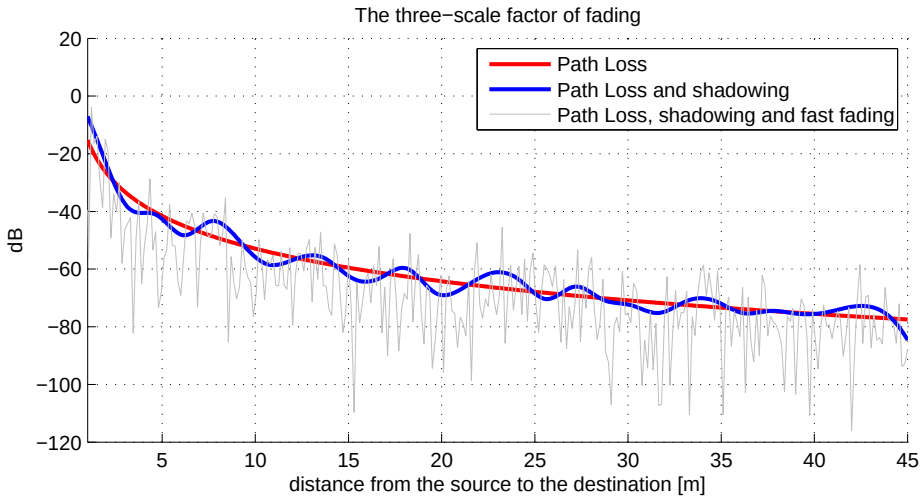

Figure 2.1: Illustation of the fading effect along the BS-MS distance

2.3.1 Small scale propagation model

Let us consider the wideband channel equation $h(\tau,t) = \sum h_n(t)\delta(\tau - \tau_n(t))$. Each path $h_n(t)$ is modeled as a continuous-time stochastic process, which means that at a fixed time t, $h_n(t)$ is the realization of a random variable that we will simply write h_n.

First-order fast-fading statistics

The channel coefficients per tap $h_n(t)$ are assumed to be the sum of M_n non-separable paths. If the number of paths is high such as $M_n \to \infty$ and the coefficients from each paths are modeled as random variables with a uniformly distributed angles of arrival and path gain. From the central limit theorem, h_n arises to have a zero mean complex Gaussian distribution, $h_n \sim \mathcal{CN}(0, 2\sigma^2_{h_n})$:

$$p(h_n) = \frac{1}{2\pi\sigma^2_{h_n}} e^{\frac{-|h_n|^2}{2\sigma^2_{h_n}}}.$$

The complex variable h_n can be decomposed into amplitude and phase terms $h_n = a_n e^{i\theta_n}$, due to the complex Gaussian distribution of h_n, a_n is Rayleigh distributed, $a_n \sim \text{Rayleigh}\,(\sigma_{h_n})$:

$$p(a_n) = \frac{a_n}{\sigma^2_{h_n}} e^{\frac{-a_n^2}{2\sigma^2_{h_n}}} \qquad a_n \geq 0$$

and θ_n is uniformly distributed over $[-\pi, \pi]$. The tap power $P_n = |h_n|^2 = a_n^2$ has an exponential distribution, $P_n \sim \text{Exponential}\left(E_n^{-1}\right)$:

$$p(P_n) = \frac{1}{E_n} e^{\frac{-P_n}{E_n}}$$

where $E_n = 2\sigma_{h_n}^2$ is the tap average power (path loss and shadowing).

It is obvious that for a flat channel which is equivalent to a single-tap channel, the whole channel h follows the same distribution, or inversely for a wideband channel, each taps have a gain which varies in time according to the standard narrowband statistics. The Rayleigh distribution is an excellent approximation to measured fading amplitude statistics for a mobile fading channel in NLOS situations. Such channels are called Rayleigh-fading channels or simply Rayleigh channels.

In a LOS situation the received signal is composed of a random multipath component, whose amplitude is described by Rayleigh distribution, plus a coherent line-of-sight component which has essentially constant power (within the bounds set by path loss shadowing). This is given by the Rice distribution for the amplitude:

$$p(a_n) = \frac{a_n}{\sigma_{h_n}^2} e^{\frac{-(a_n^2 + a_0^2)}{2\sigma^2}} I_0\left(\frac{a\, a_0}{\sigma_{h_n}^2}\right)$$

where I_0 is the zero order modified Bessel function of the first kind. Then the power is distributed as follow:

$$p(P_n|K) = \frac{(1+K)e^{-K}}{E_n} e^{(1+K)\frac{-P_n}{E_n}} I_0\left(\sqrt{4K(1+K)\frac{P_n}{E_n}}\right)$$

where K is the so called "Ricean K-factor" representing the power ration of the specular and random components.

A more general statistical model is given by the Nakagami-m distribution where the power is Gamma distributed:

$$p(P_n, m) = \frac{m^m}{E_n^m \Gamma(m)} P_n^{m-1} e^{\frac{-mP_n}{E_n}}$$

where $m \geq 1/2$ is a parameter describing the fading severity. The previously cited fading can be formulated as a specific case of Nakagami fading. The Rayleigh distribution is equal to Nakagami distribution with $m = 1$ and Rice distribution can be approximated by $m \approx \frac{(K+1)^2}{2K+1}$.

Second-order fast-fading statistics

Regarding the autocorrelation function of the fading effect, which is the inverse Fourier transform of the power spectrum density for a random process, one has a view on the effect of the Doppler spread. This function expresses the correlation between a signal at a given time and its value at some time delay, τ later. In the case of the classical spectrum with Rayleigh fading, the result is as follows:

$$\rho(\tau) = J_0(2\pi\Delta f_d \tau)$$

where J_0 is the Bessel function of the first kind and zero order and Δf_d is the maximum Doppler shift or Doppler spread, given by $\Delta f_d = f_c \frac{v}{c}$. This process leads to the definition of the coherence time T_{coh} of a channel as the time over which the channel can be assumed constant. This is assured if the normalized autocorrelation function remains close to unity for duration under consideration. The coherence time is, therefore, inversely proportional to the Doppler spread of the channel, ie $T_c \propto \frac{1}{\Delta f_d}$.

The significance of this is that signals whose duration is less than the coherence time of the channel are received approximately undistorted by the effects of the Doppler spread : Fading at two time instances separated more than the channel coherence time are uncorrelated. Usually scatterers are assumed uncorrelated, and consequently tap gain process is independently generated. If this assumption is combined with the assumption of fixed delays and fading statistics, one talks about wide-sense stationary, uncorrelated scattering (WSSUS) introduce by Bello [3].

2.3.2 Large scale propagation model

Here, in addition to the shadow fading, we introduce two other large scale parameters which exhibit similar behavior. All of these parameters appear also to be correlated between each other; this will be the object of the next chapter.

Path loss models

The path loss model predicts the average attenuation of the transmitted power along the propagation route for a specific base-to-mobile distance d. In free-space environment, the path loss L can be written as

$$PL_0(d) = \frac{P_{Rx}}{P_{Tx}} = \frac{G_{Rx} G_{Tx} \lambda^2}{(4\pi d)^2}$$

where G_{Tx} and G_{Rx} are the antenna gain at transmitter and receiver respectively. P_{Tx} and P_{Rx} are the transmitted and received power while λ is the wavelength. In decibels (dB) the relation becomes

$$PL_0(d) = P_{Rx} - P_{Tx} = L_0 - 20\log_{10} d$$

where L_o is deterministic depending on the frequency and the antenna heights.

As current communication systems do not take place in a free space, the above simple model is not directly applied, a number of different path loss models have been adapted depending on the propagation scenario studied, like the Okumura-Hata model [27,66], which is perhaps the most widely used path loss model in urban areas, or the Walfisch-Bertoni model [30], which has been adopted in the COST-231 model, an outdoor radio propagation models for applications in urban areas at 900 and 1800 MHz bands. An environment dependent exponent n is introduced:

$$PL_{dB}(d) = P_{Rx} - P_{Tx} = L_1 - 10n\log_{10} d$$

where L_1 is a constant term which depends on the antenna gains, frequency etc., usually different from that of L_0. Measurements have generalized this model for a frequency range of 2 to 6 GHz and different antenna heights. The parameter n, called the path loss exponent, is environment-specific and usually varies from 2 to 6 [56].

Shadowing

The path loss gives the expected loss of power in the local area, additionally random variations called shadow fading or shadowing, have been measured to fit almost without exception to a lognormal distribution (normally distributed in dB) [28].

The propagation loss is extended to

$$PL_{dB}(d) = P_{Rx} - P_{Tx} = L_1 + 10n\log_{10} d + X_{SF} \tag{2.4}$$

where X_{SF} is a zero mean Gaussian distributed random variable with probability density function given by

$$p(X_{SF}) = \frac{1}{\sqrt{2\pi}\sigma} e^{\frac{-X_{SF}^2}{2\sigma_{SF}^2}}$$

where σ_{SF} is the standard deviation which also is site specific. Shadow fading is the effect of physical shadowing caused by obstacles in the propagation path between the

mobile and the base station like buildings, mountains, and other objects. Numerous measurement results have been reported for different environment types since the phenomenon has been observed. Normal values for standard deviation reported in literature are between 5 to 12 dB [20].

Delay spread

Another important large scale parameter for modeling is the root mean square (rms) delay spread $\Delta\tau_{rms}$, the standard deviation of the different delay paths, which has been also measured to behave alike the path loss and shadowing with a stochastic distance dependant component and a random component. Furthermore it is lognormal distributed and correlated to the shadow fading [33]. Given an average power delay profile $\{E'_i, \tau_i\}$ for $i = 1 \dots N_{paths}$ where the power per taps has been normalized by the total channel power $E'_i = E_i / \sum_i E_i$. The rms delay spread can be simply computed as

$$\Delta\tau_{rms} = \sqrt{\sum_i \tau_i^2 E'_i - \left(\sum_i \tau_i E'_i\right)^2}. \tag{2.5}$$

As expected, the delay spread has been measured to increase with the distance as follows [33]:

$$\Delta\tau_{rms} = T_1 d^{\epsilon} y_{DS} \tag{2.6}$$

where T_1 is the median value, ϵ is an exponent that lies between $0.5 - 1.0$ and y_{DS} is a lognormal variable. Typical standard deviation of $Y_{DS} = 10 \log_{10} y_{DS}$, σ_{DS} lies from 2 to 6 dB.

Throughout this thesis, we will simply refer to the rms delay spread as the delay spread. Figure 2.2 gives an illustration of the RMS delay spread for a type of channel called a *Typical Urban channel* with a normalized total delay spread and normalized total power.

Angle spread

In the same manner, we may define the standard deviation of the angles of arrival (AOAs) of the multipath components at the receiving antenna as the angle spread at the receiver. Similarly, the angle spread at the transmitter refers to the standard deviation of the angles of departures (AODs) of the multipath that have reached the receiver. In this thesis we will only and briefly consider the angle spread at the transmitter and we will note the random variation in the log domain around

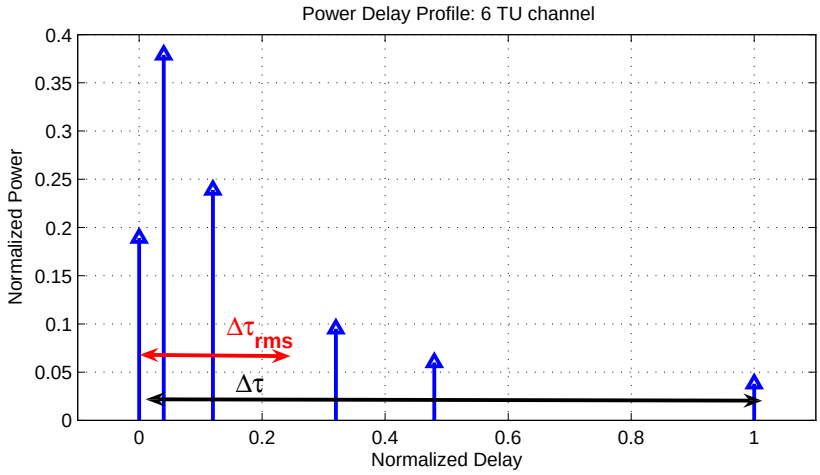

Figure 2.2: RMS delay spread on Typical Urban channel

the mean as Z_{AS}. The variable Z_{AS} has been measured as well to be Gaussian distributed [5] and its variance σ_{AS} has a typical value in the range of 1-3 dB.

Chapter 3

Correlation among large scale parameters

In this chapter we review the literature on correlation among shadow fading (SF), delay spread (DS) and angle spread (AS) for the same transmission link and different links as well. Considering a transmission from transceiver i to receiver j, we express the random variation of the SF, DS and AS, as X_{ij}, Y_{ij} and Z_{ij}, respectively. These random variables are all lognormal distributed with variance σ_{SF}, σ_{DS} and σ_{AS}. The variances are assumed independent of the transmission link for simplicity which is realistic in the case of a uniform propagation environment. Then, the correlation of two of these variables, let us say SF and AS, for two different paths ij and kl is expressed as follows

$$\rho(X_{ij}, Y_{kl}) = \frac{\mathcal{E}\{X_{ij}Y_{kl}\}}{\sigma_{SF}\sigma_{AS}}.$$

A scheme of the problem statement is depicted in Figure 3.1.

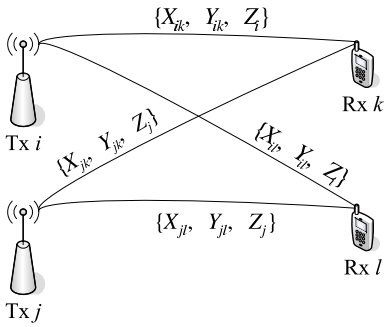

Figure 3.1: Large scale parameters of different links

3.1 Correlated shadowing

Shadowing has been analyzed to be the consequence of physical obstructions, thus signals which have crossed and been attenuated by the same obstacles are likely to present dependency. This proposal has been supported by measured correlation since the 70's [20].

Measurements campaigns and models of shadowing correlation in the literature have specially addressed the problem of correlation between links with a common node. We will distinguish two simple cases. The first case aims to depict the correlation between two close locations on a path of a moving MS, and more generally when two links from the same BS end in a different receiver. This will be called in the sequel the *shadowing auto-correlation*. Further measurements have then investigated the correlation between the two received signals at the same terminal from different source locations, often named the *shadowing cross-correlation*. A well-agreed model exists for the shadowing auto-correlation, but for the cross-correlation many models have been published and will be presented in the following. A third case of correlation between links which do not share any node in common has also been addressed recently in the literature.

Correlations between links could have a significant effect on the performance of a system. The lognormal shadowing from two different below rooftop RSs at a given MS location will have some level of correlation. In addition, the shadowing components from a given RS site at two different MS locations will be correlated if they are within the spatial de-correlation distance of the shadowing. In order to correctly model the benefits of relaying this correlation needs to be taken in account. Nevertheless, the auto-correlation can be assumed negligible if receivers' locations are far enough, but a certain amount of cross-correlation is often measured even if the BSs are far from each other. The reason is that the shadowing results mainly from obstructing objects closely surrounding the terminal. Thus, even if they arise from the same causes, auto-correlation and cross-correlation are modeled differently.

Let us call X_{ij} the shadow effect from transmitter i to receiver j. In a uniform propagation environment, the same values of shadowing standard deviation will be assumed for all links, thus the correlation for the two different paths, ij and kl, is expressed as follows

$$\rho_{ij,kl} = \frac{\mathcal{E}\{X_{ij}X_{kl}\}}{\sigma_{SF}^2}.$$

As an example, $\rho_{ij,kj}$ is the cross-correlation between transmitter i and k at receiver j; and $\rho_{ij,il}$ is the auto-correlation between receiver j and l from transmitter i. In

the following, if there is no confusion for receiving terminal j this cross-correlation will be simply expressed as ρ_{ik}; and if there is no confusion for the transmitter this auto-correlation will be denoted by ρ_{jl}.

3.1.1 Auto-correlation models

Several measurements fields have suggested that an exponential decaying function is an appropriate model for the auto-correlation function of the shadow fading [24, 35]. The model is characterized by the so-called shadowing decorrelation distance d_c:

$$\rho_{jl} = e^{-\frac{\Delta_{jl}}{d_c}} \tag{3.1}$$

where Δ_{jl} is the distance between receiver j and receiver l. The decorrelation distance d_c is typically a few tens or hundreds of meters depending how far the receivers are from the BS [35, 56].

The above model suggests that the shadowing process is a first order Markovian process [15], which can be generated easily. A modification of this model which complies with the level crossing theory of a Gaussian process is proposed in [17]. Some other studies proposed to generalize the model by a composite of two exponential functions in order to match better some measurements [5, 57].

3.1.2 Cross-correlation models

The shadowing cross-correlation represents the correlation among the shadow effect of different links merging at the same receiver but emerging from different transmitters. Since cross-correlation has been early evidenced in the work by Graziano in 1978 [20], several measurement campaigns have been carried out in order to catch the physical behavior as well as to derive mathematical modeling [6,46,61,69]. Field measurements were performed under a different environment supporting the intuitive conjecture that links with a common terminal are in general correlated. Arnold et al. [6] studied this issue in the context of macrodiversity gain, analyzing 800 MHz data collected in a residential environment with indoor and outdoor transmitters for a single mobile receiver. Interestingly, some field measurements failed to bare significant correlation. In [46], data were obtained from a 1900 MHz GSM system in rural and suburban areas, in both environments the measured correlation was relatively low, ranging even in the negative value in rural areas. The authors specified that the negative correlation was from a particular drive route and BS locations of a specific site. They also investigated the dependency of the cross-correlation on the

angle between the mobile and the cell sites, but no dependency was found.

The primary models consist of empiric tables from measurements. More recently, more elaborated model using analytic functions have been derived. On the other hand, despite the fact that field tests have suggested that the cross-correlation has a decisive effect upon the system performance, cross-correlation is often set to zero in system simulations avoiding complication of the analysis. It has been shown, for example, that cross-correlation effects cannot be ignored in the performance analysis of the co-channel interference probability for microcellular and picocellular systems [70]; it also has a significant impact on the rates of level crossings [39]. In [68], the authors evaluate the performance of downlink in hard handover and soft handover based CDMA cellular systems for different shadowing correlation models and show that different correlation models lead to different simulation performances. They analyze also the impacts of cross-correlated shadowing on the soft handover gain in downlink through simulations in a UMTS (Universal Mobile Telecommunications System) vehicular environment. Handoff performance with cross-correlation of the shadowing process was also analyzed by Viterbi in [62]. In [63], Viterbi *et al.* has also modeled cross-correlation in the interference evaluation for CDMA cellular networks. Ignoring correlation could lead to pessimistic results while predicting mobile systems performance through simulations according to [69].

Physical basis and modeling

Empirical measurements have supported the modeling of shadowing component as a lognormal variation around the path loss. This variation is known to be largely determined by the surrounding terrain at the terminal location and by obstructing objects in close proximity to the MS.

An extension of this model in order to introduce dependency between link attenuations is to break the shadowing effect into two independent components [6,63]. The first component is dependent of the near field of the receiver and thus common for all signals from different BSs; the second component depends of terrain and obstucting objects belonging exclusively to a specific BS-MS link. Second components among different links are assumed uncorrelated. This model, first suggested by Arnold *et al.* in 1988 [6], was shown to well match the measured data for outdoor to indoor links having similar length. In other words the random component of the dB loss for the ith base station is expressed as:

$$X_i = \sqrt{\rho}\xi + \sqrt{1-\rho}\xi_i \tag{3.2}$$

such that ξ and ξ_i are uncorrelated zero-mean Gaussian variables of the same variance σ^2_{SF}; the component ξ_i, ξ_j from BSs i and j are independent for all i and j, $i \neq j$.

The normalized covariance (correlation coefficient) of the losses to two base stations, i and j, is $\frac{\mathcal{E}[X_i X_j]}{\sigma^2_{SF}} = \rho$. This model includes the limiting cases of independent attenuations ($\rho = 0$) and of highly correlated attenuations ($\rho = 1$), which might apply when the mobile is completely shadowed in all directions. In [63], the authors chose the reasonable assumption that the two random components have equal standards deviations in which case the normalized covariance is $\rho = 1/2$ for all pairs of base stations. This assumption is widely used in literature and in many standards such as 3GPP. This special case of a constant correlation model may reasonably approximate closely spaced base stations in a circular array [70].

Because the two random components have the same contribution in every link, this model induces a constant correlation between all the links. A more general model was developed by Graziosi *et al* in 1999 [21] based on the work of Viterbi where the shadowing is a sum of multiple components having different contributions.

$$X_i = \sum_m \sqrt{\rho_{im}}\xi_{im} \text{ where } \sum_m \rho_{im} = 1 \tag{3.3}$$

Modeling the shadowing as the sum of different random variables, some being correlated, does not say much about the level of correlation. Two channels links crossing common obstacles should suffer similar attenuation. In order to introduce a dependency in the statistical model of the shadowing component, we must estimate the amount of correlation. The terrain of propagation of the link is the key factor in the amount of correlation, for example in [69], the authors noticed that the streets orientation has an influence on the measurements. Parallel streets to the base stations axis imply a higher correlation than orthogonal ones to this same axis. Without knowing the exact terrain of the transmission, we can assumed that spatially-close links should cross the same kind of obstacles. In order to determine the amount of common routes for the two links, two key variables have been investigated: the angle-of-arrival difference θ_{ij} which represents the angle between the two paths from different base stations to the mobile and the relativity of the two path lengths $R_{ij} = \frac{r_i}{r_j}$, for $r_i \leq r_j$ [32, 56]. When the angle-of-arrival difference is small, the two path profiles are assumed to share many common elements and are expected to have high correlation. On the other hand, as the longer path length increases, it incorporates more elements, which are not common to the shorter path; therefore, the correlation decreases. These issues have been recognized by many researchers

and, in particular, those interested in macrodiversity (for example, see [6] and [20]).

In most cases, the correlation is considered as a function of θ_{ij} only [20,21,37,58], because the angle-of-arrival difference has the strongest influence on the results. The dependence of the correlation function on θ_{ij} is suggested by the measurements conducted by Zayana and Guisnet [69] in two French cities, and also by previous measurements reported in [20] and [61]. In [20], Graziano measures the correlation of the signals as a function of angle using data at 900 MHz using data from two sets of transmitters. Using this relatively limited data set, Graziano observed correlations on the order of 0.6 to 0.8 at angles less than about 10 degrees. In [6], the authors observed that the macroscopic diversity gain is more significant for links well separated in angle. The fact that links from relatively close directions should be strongly correlated was assumed by Bell Laboratories' researchers in [18,25], for this they designed a correlation function on the angle-of-arrival difference; the same model being developed later and independently by Graziosi [21].

On the contrary, from a measurements field in Boston (urban and suburban terrain) at 1900 MHz [65], the authors did not find significant dependency from the angle-of-arrival even for small angles. They argue that the data set used by Graziano [20] was relatively limited and collected only on a relatively flat terrain. They finally concluded that the correlation should be low even at small angles, if the length of terrain causing shadowing which is not common to the two paths is larger or on the same order as the terrain distance that is common to the two paths. This last observation is taken in account with the other key variable R_{ij} introduced by Zayana and Guisnet in 1998 [69]. From a set of measurements and simulations, Zayana and Guisnet [69] proposed a model where the cross-correlation depends upon two variables: the angular separation between the two base stations as seen from the mobile and the ratio between the distances from the mobile to the base stations.

From this, in 2001, Avidor [7, 39] suggests that the correlation can be modeled as the product of two functions: $\rho_{ij} = g(\theta_{ij}) \times h(R_{ij})$,where g and f should be positive-definite functions with maximum at zero, and g even and 2π-periodic. The authors provided potential candidates in [7].

Constant correlation model

A constant cross-correlation of 0.5 is the adopted value in [2]. As mentioned above, this particular model is suggested by the measurements in [6] and assumed, for example, in [63, 70].

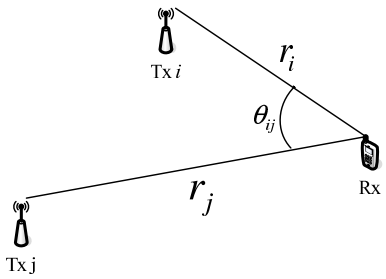

Figure 3.2: Physical model for shadowing cross-correlation

Graziosi model

In [21], the model of Equation (3.2) [63] is generalized with the will to introduce dependency of the angle-of-arrival differences θ_{ij}. On the basis of experimental results of [69], and also previous measurements reported [20], the authors designed the correlation as an even, periodic function:

$$\rho_{ij} = A\cos(\theta_{ij}) + B, \tag{3.4}$$

with A, B positive real constants and $A + B \leq 1$. The previous constant cross-correlation model can be obtained with $A = 0$ and $B = 0.5$.

This correlation model has been used earlier by Bell Laboratories researchers in the context of capacity simulations [18, 25], and independently by Graziosi *et al.* [21] in the analysis of handoff. In [25], with the lack of field measurements, the following specific case was chosen : $p_{ij} = 0.699 + 0.3\cos\theta_{ij}$. In a later work, $\rho_{ij} = 0.5 + 0.3\cos\theta_{ij}$ was chosen [40].

Zayana and Guisnet measurements and model

Zayana and Guisnet [69] have supervised a measurements campaign in order to develop an empirical model for the cross-correlation. The measurements were conducted at 900MHz in a small urban environment in a French city. They have studied the effect of the angular separation between BS-MS links on the cross-correlation and also the effect of the ratio between the link lengths expressed in dB $R_{ij}^{dB} = 10\log_{10} R_{ij}$. As expected, their results show strong correlation between links with small angular separation, which decreases when the angular separation grows. And simulations with PARCELL (which is a France Telecom radio cellular engineer-

ing tool) results that the cross-correlation falls, for a fixed angle, when module R_{ij}^{dB} grows. The model is expressed by the table below:

$\rho(\theta, R)$	$\theta \in [0°; 30°]$	$\theta \in [30°; 60°]$	$\theta \in [60°; 90°]$	$\theta \geq 90°$
$R_{dB} \in [0; 2]$	$\rho = 0.8$	$\rho = 0.5$	$\rho = 0.4$	$\rho = 0.2$
$R_{dB} \in [2; 4]$	$\rho = 0.6$	$\rho = 0.4$	$\rho = 0.4$	$\rho = 0.2$
$R_{dB} \geq 4$	$\rho = 0.4$	$\rho = 0.2$	$\rho = 0.2$	$\rho = 0.2$

Linear models

The publication [32] extends the work of Zayana and Guisnet by taking the table of result of [69] and comparing with other experimental results from [20,36,58]. The model is a linear variation between the different experimental values. They provide different models with or without taking account of the ratio of distance of the path links:

– *Model 0.8/0.4* approximates the measurement results by Graziano [20]:

$$\rho(\theta) = \begin{cases} 0.8 - \frac{\theta}{150} & \text{if } \theta \leq 60° \\ 0.4 & \text{if } \theta > 60° \end{cases} \tag{3.5}$$

– *Model 0.8/0.0* approximates the measurement results by Sorensen [58]:

$$\rho(\theta) = \begin{cases} 0.8 - \frac{\theta}{75} & \text{if } \theta \leq 60° \\ 0.0 & \text{if } \theta > 60° \end{cases} \tag{3.6}$$

– *Model 1.0/0.4 RX*:

$$\rho(\theta, R) = \begin{cases} f(X, R)(0.6 - \frac{\theta}{150}) + 0.4 & \text{if } \theta \leq 60° \\ 0.4 & \text{if } \theta > 60° \end{cases} \tag{3.7}$$

– *Model 1.0/0.0 RX*:

$$\rho(\theta, R) = \begin{cases} f(X, R)(1.0 - \frac{\theta}{75}) & \text{if } \theta \leq 60° \\ 0.0 & \text{if } \theta > 60° \end{cases} \tag{3.8}$$

where

$$f(X,R) = \begin{cases} 1 - \frac{R}{X} & \text{if } R \leq X\text{dB} \\ 0 & \text{if } R > X\text{dB} \end{cases} \tag{3.9}$$

and X denotes the point where the distance-dependent correlation reaches its minimum value. The authors assumed that X is in the range of 6-20dB.

Saunders model

In [56], the following cross-correlation model is proposed:

$$\rho(\theta, R, r_i) = \begin{cases} \sqrt{R} & \text{for } 0 \leq \theta \leq \theta_T \\ \left(\frac{\theta_T}{\theta}\right)^{\gamma} \sqrt{R} & \text{for } \theta_T \leq \theta \leq \pi \end{cases} \quad \text{with } \theta_T = 2 \arcsin \frac{d_c}{2r_i} \tag{3.10}$$

where γ is a parameter depending of the terrain and d_c is the auto-correlation distance which is the distance taken for the normalized auto-correlation to fall below $1/e$.

It is worthy to notice that this is the only model taking in account both value r_i and r_j rather than just its ratio.

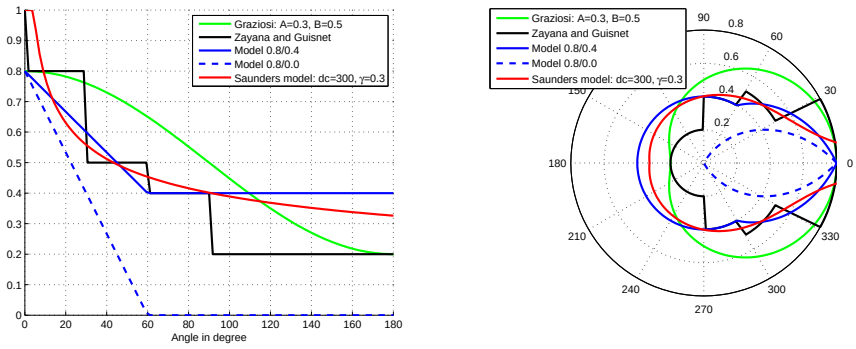

(a) Cartesian plot

(b) Polar plot

Figure 3.3: Angular behavior of the different shadowing cross-correlation models ($R_{dB} = 0$).

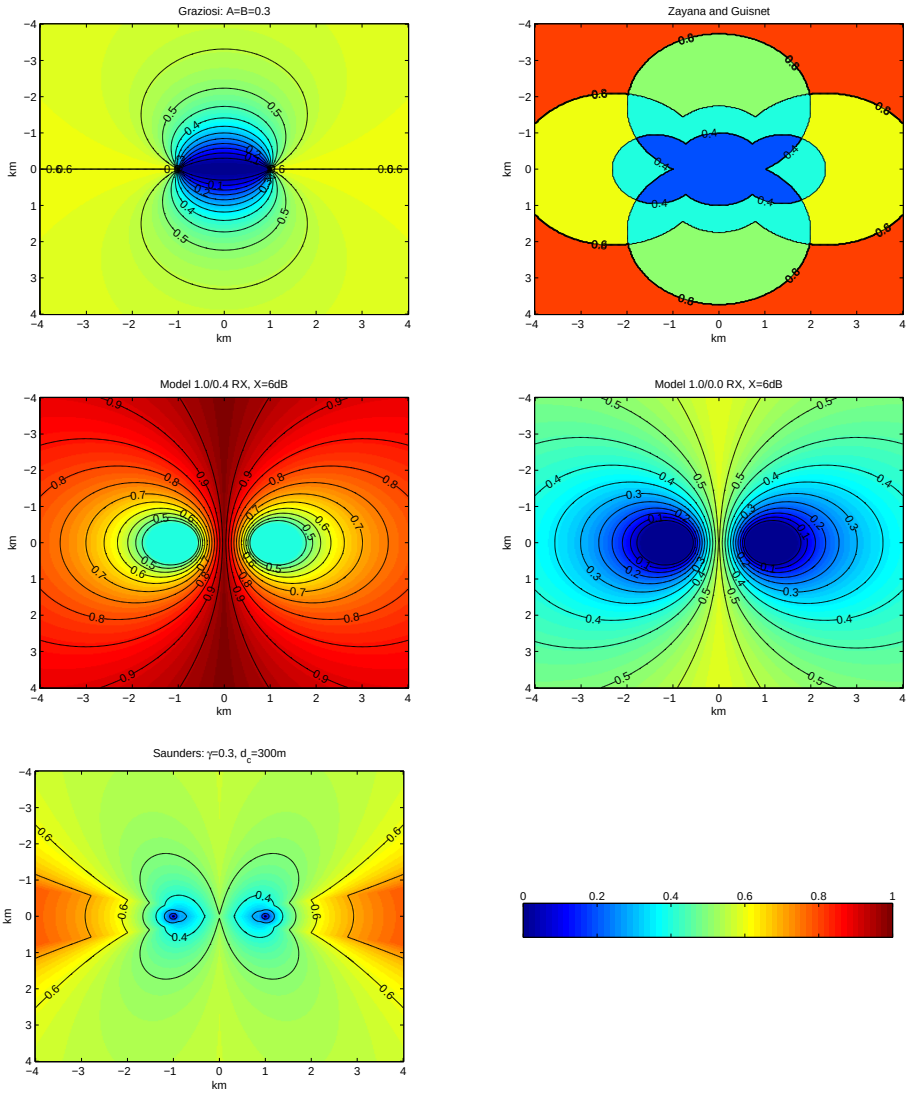

Figure 3.4: Exemplification of different shadowing cross-correlation models between two BSs distant of 2km.

3.1.3 Correlation among links without a common node

The correlation among links without a common node haa been recently studied in the literature [22, 67]. In [67], the correlation is modeled by an exponential function of the distances between the receivers and transmitters. In [22], the correlation is generated by multiplying the auto-correlation and cross-correlation. This method was also used in [21, 69], see also [31]. The authors of [22] attempt to rigorously prove that combining of auto- and cross-correlation is done by multiplication. The proof is unfortunately weak, by taking independent increment to model the random variable; the authors implicitly assumed that the model is Markovian which results by a multiplication of the correlation.

3.2 Correlated angle spread, correlated delay spread

Angle spread (AS) and delay spread (DS) have been shown to be also lognormal distributed. Contrary to the shadow fading, auto- and cross-correlation of AS and DS for different transmission links have raised little interest in the literature. Nevertheless, auto-correlation of AS and auto-correlation of DS seem to follow also an exponential decaying with different decorrelation distances than the shadow fading [5, 42]. Angle-spread and delay spread fluctuations between different base stations (cross-correlation) have been assumed to be uncorrelated due to the lack of investigation. Some measurement fields can be found in [42]. In [42], the authors conclude that when the BSs are close, the angle spread is correlated but less significantly than the shadow fading and can be thus neglected.

3.3 Correlation among the "three spreads"

In the literature shadow fading, angle spread and delay spread have been measured to be correlated among each other [5] (for the same transmission link). Greenstein [33] presents a significant model which results in negative correlation between delay spread and lognormal shadow fading. In some standard channel models, the following values of the cross-correlations between path-loss, delay spread and angle spread for the same base station have been adopted [23] from [12]:

- Correlation between shadowing and delay spread: $\rho_{XY} = -0.75$
- Correlation between shadowing and angle spread: $\rho_{XZ} = -0.75$
- Correlation between delay spread and angle spread: $\rho_{YZ} = 0.5$

The associated correlation matrix is:

$$\boldsymbol{A} = \begin{pmatrix} 1 & \rho_{XY} & \rho_{XZ} \\ \rho_{XY} & 1 & \rho_{YZ} \\ \rho_{XZ} & \rho_{YZ} & 1 \end{pmatrix}. \tag{3.11}$$

The problem of correlation between the large scale parameters of different links have not been investigated, but it is to expected that these correlations are negligible.

3.4 The problem of a positive definite correlation matrix

In this section, we consider M links merging at the same receiver. Assuming that the random variation of the large scale parameters (SF,DS,AS) of all links are jointly Gaussian in the log-domain, they should thus possess the proper statistical characteristic that the full correlation matrix for the M BSs is positive semidefinite. As a first step we will only discuss the problem for shadow fading. In this section, as the statement of the problem suggests, we only consider the cross-correlation, nevertheless the auto-correlation model of (3.1) leads to a positive correlation matrix due to its inherent Markovian assumption.

3.4.1 Cross-correlation model

For a given network of BSs with one MS, a correlation matrix $\boldsymbol{R_{xx}}$ of the shadowing for every transmission link has to be calculated for simulation. If a vector of independent lognormal samples are generated at a given MS location, representing the shadowing from each BS, then these samples can be correlated using $\boldsymbol{R_{xx}}$.

Most of the cross-correlation models have the main drawback to randomly lead to a non positive semidefinite matrix which is a necessary condition for a matrix to be a correlation one. Surprisingly, many authors assumed de facto the positive-definiteness and state that the Cholesky decomposition can be applied, this property is, of course, totally dependent on the way of choosing the entries of the aforesaid matrix. However, this important feature has been recognized, for example, in [7, 21, 40, 68]. In [21], the authors provided a proof that their model leads to a positive-definite correlation matrix relying on a Fourier series expansion (provided also for a more general class of cross-correlation laws). In [7], the authors extend the work of Zayana and Guisnet by determining different correlation function using the fact

that the covariance matrix must be positive definite. By using the assumption those covariances can be separated into the product of two terms that depend only on the angular difference and the ratio of distances respectively, one can write

$$\rho(X_{ij}, X_{kj}) = g(\theta_{ik})h(R_{dB}^{ik})$$

It follows that g and h are even, positive-definite functions with the maximum at zero and g has a period 2π. Since g is even and periodic, it can be written as a Fourier series $g(\theta) = \sum_{n=-\infty}^{\infty} c_n e^{jn\theta}$, where the Fourier coefficients c_n are all real. Using measure theory and applying Bochner's theorem, the authors show that g is positive definite if and only if $\forall n\, c_n \geq 0$ and $0 < \sum_{n=-\infty}^{\infty} c_n < \infty$. It is sufficient for h to be convex on the right half-axis $[0, \infty)$ to be positive definite. Then the product of g and h is positive definite on $[-\pi, \pi] \times \mathbb{R}$ by Schur's Theorem. The authors leave the specific shape of the function h open and note that this decomposition in two functions which are independent may not be the best.

We summarize in the table below which of the models described previously fulfill this requirement.

Model	Always leading to a semi-positive matrix
constant $\rho = 0.5$	yes
Graziosi	yes [21]
Zayana and Guisnet	no
linear models	no
Saunders model	no

3.4.2 Overall model

When generating the three spreads for a network of M base stations, the problem of non-negative correlation matrix is complicated drastically. Given a link the correlation among the three spread is given according to the matrix $\boldsymbol{A}$ (3.11), which is positive definite with the adopted value. On the other hand, the correlated shadowing is represent by $\boldsymbol{R_{xx}}$. When accounting the entire variable together we must define the cross-correlation of the AS and DS, as well as the correlation among all the spread for the different links. The latter correlations are often assumed to be zero, which leads to non semi-positive definite overall matrix in most of the cases

even if $\boldsymbol{A}$ and $\boldsymbol{R_{xx}}$ are non negative definite. In [38], assuming that the shadowing cross-correlation is constant and equal to 0.5, the authors proposed as a solution to modify the entries of the matrix A in order to force the overall eigenvalue to be positive. The adopted new values can be found in [10]:

- Correlation between shadowing and delay spread: $\rho_{XY} = -0.6$
- Correlation between shadowing and angle spread: $\rho_{XZ} = -0.6$
- Correlation between delay spread and angle spread: $\rho_{YZ} = 0.5$

Nevertheless, for another type of shadowing cross-correlation model, no other solution exists. Alternatively, without any experimental backing, we may assume that the shadowing cross-correlation model may apply to the other large scale parameter and the overall correlation matrix can be obtain by a Kronecker product between $\boldsymbol{A}$ and $\boldsymbol{R_{xx}}$: $\boldsymbol{A} \bigotimes \boldsymbol{R_{xx}}$. Then by the properties of the Kronecker product, the overall matrix is positive semidefinite if $\boldsymbol{A}$ and $\boldsymbol{R_{xx}}$ are.

Chapter 4

OFDM

Orthogonal frequency-division multiplexing (OFDM) is a widely used modulation technique in current and future wireless standards. OFDM is a multichannel modulation that sends multiple symbols in parallel, by dividing the given channel into many narrow subchannels called subcarriers. A good overview of OFDM can be found in [29].

Multichannel modulation systems have been studied since the middle of the 20^{th} century. Its relevance has been contested until the use of discrete Fourier transform (DFT) with a cyclic prefix. Fast Fourier transform (FFT) makes the implementation of DFT efficient, and the cyclic prefix brings robustness against inter-symbol, inter-carrier interference (ISI, ICI) and fading caused by multipath propagation.

In the following sections of this chapter, the principles of the OFDM transmission technique will be described with a short performance analysis.

4.1 Principles of OFDM

OFDM is a block transmission technique where complex-valued data symbols are not modulated by using the full allocated radio resource, but are parted into different low-rate data streams modulated by different narrow baseband carriers. The transmitted OFDM signal is the sum of all the subcarriers which are chosen orthogonal. The main advantage of this concept is that in a frequency selective channel, the channel for each of the subcarrier can be considered flat. In a time-invariant fading channel, ISI and ICI can be avoided with a cyclic prefix.

In the baseband domain, an OFDM block signal consists of N orthogonal subcar-

riers $\phi_k(t)$ modulated by parallel streams of complex data symbol $\{x_k\}$:

$$s(t) = \frac{1}{\sqrt{N}} \sum_{k=0}^{N-1} x_k \phi_k(t), \qquad 0 < t < NT$$

where NT is the length of the OFDM block. Each baseband subcarriers are designed to be orthogonal on $0 < t < NT$:

$$\phi_k(t) = e^{j2\pi f_k t}$$

where the subcarrier frequencies are equally spaced $f_k = \frac{k}{NT}$.

The left half of Figure 4.1 illustrates three different subcarriers in time, the right half of Figure 4.1 illustrates the orthogonality of the subcarriers in the frequency domain and the resulting total spectrum.

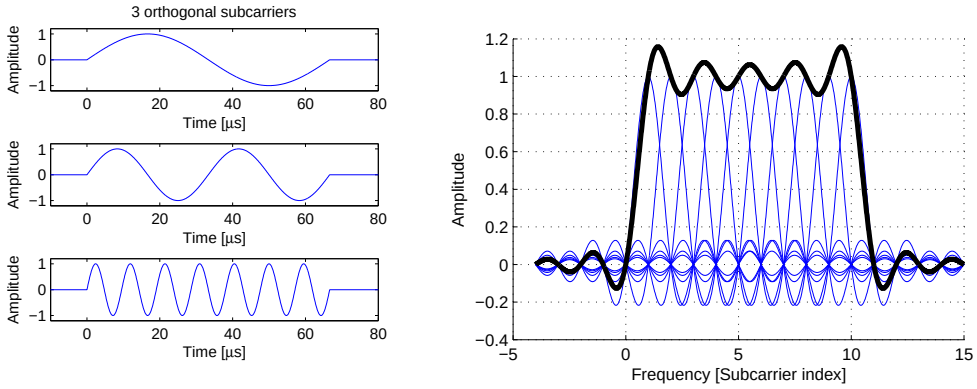

Figure 4.1: Subcarriers in time and frequency

At the receiver side, the signal is sampled (here the fading and the noise is ignored):

$$s(nT) = \frac{1}{\sqrt{N}} \sum_{k=0}^{N-1} x_k e^{j2\pi \frac{nk}{N}}, \qquad 0 < n < N-1.$$

From this equation we can see that the OFDM symbols can be expressed in terms of an inverse discrete Fourier transform (IDFT), and can be easily demodulated via a DFT, which make the implementation of OFDM very attractive using the fast Fourier transform algorithm.

However, if we consider that the signal has been sent through a multi-tap channel and the transmitter sent successive OFDM blocks, the dispersion of the channel creates ISI between the OFDM blocks as well as ICI between the modulated data

after DFT due to a loss of orthogonality. The insertion of a guard interval (zero padding) between successive OFDM blocks would avoid ISI but it does not avoid the loss of the subcarrier orthogonality. Replacing the guard interval by a cyclic prefix (CP) - see Figure 4.2 - solves the problem and prevents both ISI and loss of orthogonality between the subcarrier if the length of the CP is greater than the delay spread of the channel.

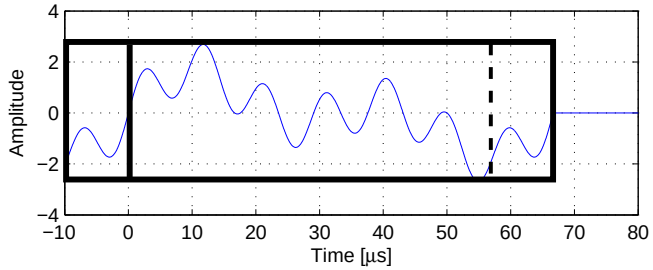

Figure 4.2: Cyclic Prefix

Now, the OFDM block $s(t)$ can be extended over a period Δ so that

$$s(t) = \frac{1}{\sqrt{N}} \sum_{k=0}^{N-1} x_k e^{j2\pi f_k t}, \qquad -\Delta < t < NT.$$

The signal then suffers from multipath propagation $h(\tau) = \sum_{i=1}^{N} h_i \delta(\tau - \tau_i)$ with a maximum delay spread $\Delta\tau$. If the length of the CP Δ is chosen such that $\Delta > \Delta\tau$, the received OFDM block evaluated on the interval $[0, NT]$, ignoring any noise effects, becomes:

$$r(t) = (h * s)(t) = \frac{1}{\sqrt{N}} \sum_{k=0}^{N-1} H_k x_k e^{j2\pi f_k t}, \qquad 0 < t < NT \tag{4.1}$$

where

$$H_k = \int_0^{\Delta\tau} h(\tau) e^{j2\pi f_k \tau} \mathrm{d}\tau$$

is the Fourier transform of $h(t)$ evaluated at the frequency f_k. It is noticeable that the data have been attenuated by the channel but the orthogonality of the subcarrier has been preserved.

Equation (4.1) suggests that the OFDM signal can be still be demodulated by a DFT on the interval $[0, NT]$, after dropping the CP. The received data then has the

form

$$y_k = H_k x_k, \qquad k = 0, \ldots, N-1$$

This is equivalent to a transmission of parallel data streams through flat channels.

4.2 Performance analysis

In practice, the CP is rarely long enough to cover the maximum delay spread of the channel and completely prevent ICI/ISI. In consequence, interferences from other symbols transmitted in the considered block (ICI) and all other symbols transmitted in other blocks (ISI) occur and lead to a loss in per-subcarrier signal-to-interference and noise ratio (SINR).

Denoting $x_{i,n}$ the nth symbol of the ith block ($0 \leq n \leq N-1$, $-\infty < i < +\infty$), the ith transmitted block with CP contains $N+\nu$ time-domain samples, of which the mth sample, for $-\nu \leq m \leq N-1$, is given by

$$s_i[m] = \frac{1}{\sqrt{N}} \sum_{l=0}^{N-1} x_{i,l} e^{j2\pi \frac{lm}{N}}. \tag{4.2}$$

Given a continuous-time channel $h(\tau)$, we may associate the corresponding discrete-time channel $h[l] = h(lT)$ where T is the sampling period. Assuming an infinite-taps, time-invariant, discrete-time channel $h[l] = \sum_k h[k]\delta_{l-k}$, for each transmitted block of $N+\nu$ samples, the receiver selects N consecutive samples and drops the other ν samples. The remaining samples $r[k]$ of the jth block, assuming perfect synchronization between the receiver and the transmitter, given for $k = j(N+\nu), \cdots, j(N+\nu)+N-1$ by

$$r[k] = \sum_{i=-\infty}^{+\infty} \sum_{m=-\nu}^{N-1} s_i[m] h[k - m - i(N+\nu)] + n[k] \tag{4.3}$$

are demodulated using a DFT. For the block $j = 0$, the nth output of the DFT can be written as

$$y[n] = x_{0,n}\mathcal{H}_{n,n,0} + \underbrace{\sum_{\substack{l=0 \\ l\neq n}}^{N-1} x_{0,l}\mathcal{H}_{l,n,0}}_{ICI} + \underbrace{\sum_{\substack{i=-\infty \\ i\neq 0}}^{+\infty} \sum_{l=0}^{N-1} x_{i,l}\mathcal{H}_{l,n,i}}_{ISI} + \tilde{n}[n] \tag{4.4}$$

where $\tilde{n}$ is the post-processed noise with power N_0, and

$$\mathcal{H}_{l,n,i} = \frac{1}{N} \sum_{m=-\nu}^{N-1} \sum_{k=0}^{N-1} h[k-m-i(N+\nu)] e^{j2\pi \frac{lm-kn}{N}}$$

denotes the signal component at the nth DFT output during the block $j = 0$, caused by the symbol $x_{i,l}$ which is transmitted on the lth carrier during the ith block. As an example, by substituting the summation variable $r = k - m$ in $\mathcal{H}_{n,n,0}$, we may write

$$\mathcal{H}_{n,n,0} = \sum_{r=-\infty}^{\infty} c[r] h[r] e^{-j\frac{2\pi nr}{N}} \tag{4.5}$$

where $c[r]$ is a weight function defined as

$$c[r] = \begin{cases} \frac{N+r}{N} & -N \le r < 0 \\ 1 & 0 \le r < \nu \\ \frac{N-(r-\nu)}{N} & \nu \le r < N+\nu \\ 0 & \text{elsewhere} \end{cases}.$$

We thus see that in the case of a causal channel $h[r] = \sum_{k=0}^{N_h} h[k]\delta_{r-k}$ where the last tap index is in less or equal than the CP length, $N_h \le \nu$, $\mathcal{H}_{n,n,0} = \sum_{r=0}^{N_h} h[r] e^{-j\frac{2\pi nr}{N}}$ is the Fourier transform of the channel evaluated at the n subcarrier.

Assuming the data symbols are statistically independent and have an average energy of σ_x^2, i.e., $\mathcal{E}\left[x_{i,n} x_{j,k}^*\right] = \sigma_x^2 \delta_{ij} \delta_{nk}$, the instantaneous SINR of the nth subcarrier is

$$\gamma(n) = \frac{|\mathcal{H}_{n,n,0}|^2}{\sum\limits_{\substack{l=0 \\ l\neq n}}^{N-1} |\mathcal{H}_{l,n,0}|^2 + \sum\limits_{\substack{i=-\infty \\ i\neq 0}}^{+\infty} \sum\limits_{l=0}^{N-1} |\mathcal{H}_{l,n,i}|^2 + N_0/\sigma_x^2}. \tag{4.6}$$

The instantaneous SINR may be used to express the corresponding ergodic capacity of the system:

$$\mathcal{C} = \sum_n \mathcal{C}(n) = \sum_n \mathcal{E}\left[\log(1+\gamma(n))\right]. \tag{4.7}$$

Applying Jensen's inequality due to the concavity of the logarithm, we have the following upper bound:

$$\mathcal{C} \le \sum_n \log(1 + \mathcal{E}\left[\gamma(n)\right]). \tag{4.8}$$

The average of the instantaneous SINR, $\mathcal{E}[\gamma(n)]$, may be hard to find as it implies the ratio of dependent random variables. In order to simplify the performance analysis, rather than using the expectation of the instantaneous SINR, we will use as an approximation the ratio between the average of the useful signal power and the average interference plus noise power. Rewriting $\gamma(n) = \frac{\mathcal{S}(n)}{\mathcal{I}(n)+N_0/\sigma_x^2}$, where $\mathcal{S}(n)$ and $\mathcal{I}(n)$ are dependent random variables, from the definition of the covariance of two random variable we have

$$\mathcal{E}[\gamma(n)] = \frac{\mathcal{E}[\mathcal{S}(n)]}{\mathcal{E}[\mathcal{I}(n)] + N_0/\sigma_x^2} - \frac{\mathrm{Cov}[\gamma(n), \mathcal{I}(n)]}{\mathcal{E}[\mathcal{I}(n)] + N_0/\sigma_x^2}. \tag{4.9}$$

As the ratio $\Gamma = \frac{\mathcal{E}[\mathcal{S}(n)]}{\mathcal{E}[\mathcal{I}(n)]+N_0/\sigma_x^2}$ has already been calculated in closed-form [59] and shown to be independent of the subcarrier index if all the carriers are modulated, for simplicity we assumed that $\Gamma \approx \mathcal{E}[\gamma(n)]$ which gives an approximation of the capacity as follows

$$\mathcal{C} \lessapprox N \log(1+\Gamma). \tag{4.10}$$

An exact derivation of the performance metric Γ has been provided for a time-varying, frequency-selective, discrete-time channel in [59] and for a continuous time channel in [41]. In this thesis, as in [8], we will only consider a time-flat channel and we will use the simplified expression of the SINR Γ of [8] for a continuous time channel. Given a channel $h(\tau) = \sum_i h_i \delta(\tau - \tau_i)$ with complex gains per taps h_i, we note the average power of every taps by $E_i = \mathcal{E}\left[|h_i|^2\right]$. The useful signal power and interference power are independent of the subcarrier index and equal to

$$P_{\mathcal{S}} = \mathcal{E}[\mathcal{S}] = \sum_i c(\tau_i)^2 E_i \tag{4.11}$$

$$P_{\mathcal{I}} = \mathcal{E}[\mathcal{I}] = \sum_i (1 - c(\tau_i)^2) E_i \tag{4.12}$$

where $c(\tau)$ is a bias function defined as follows:

$$c(\tau) = \begin{cases} 0 & \tau < -NT \\ \frac{NT+\tau}{NT} & -NT \leq \tau < 0 \\ 1 & 0 \leq \tau < \Delta \\ \frac{NT-(\tau-\Delta)}{NT} & \Delta \leq \tau < NT + \Delta \\ 0 & NT + \Delta \leq \tau \end{cases}$$

with T the sample interval in seconds, N the FFT length in samples, so the OFDM symbol interval is NT. The CP length is $\Delta = \nu T$ seconds and the combined length of the OFDM symbol and the CP is $NT + \Delta$. The biased function is depicted in Figure 4.3. Finally the SINR, Γ, may be expressed by

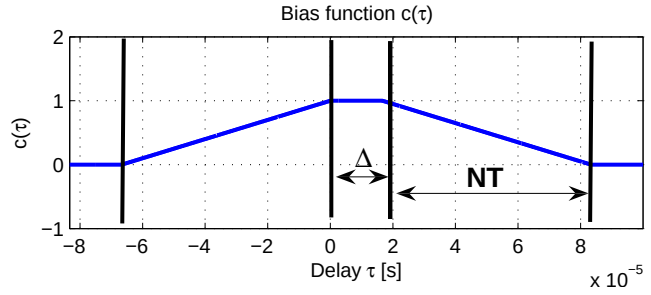

Figure 4.3: Bias function

$$\Gamma = \frac{P_{\mathcal{S}}}{P_{\mathcal{I}} + N_0/\sigma_x^2}. \tag{4.13}$$

The average SINR may be expressed in the same manner for a discrete-time channel using the equivalent discrete bias function $c[r]$.

In the following, we will refer to "average SINR" as the ratio of the average useful signal power onto the average interference plus noise power, Γ.

4.3 Time of reference

Timing synchronization is an important aspect for OFDM systems. The OFDM receiver is assumed to remove the CP and demodulate the data only over the symbol interval NT. At the receiver side, when performing the demodulation (FFT), a synchronization error may occur and degraded as well the performance of the OFDM system. We will call this synchronization instant the time-of-reference (TOR). Several OFDM timing algorithms have been analyzed, e.g., in order to choose the TOR that minimize the overall interference power and thus maximize the SINR [11, 59].

In fact the SINR expression (4.13), Γ, may be expressed simply as a function of the TOR. During the demodulation, if the FFT starts at time t_{or}, the resulting

post-FFT average signal and interference power per subcarrier are given by [8]:

$$P_{\mathcal{S}}(t_{or}) = \sum_i c(\tau_i - t_{or})^2 E_i \quad (4.14)$$

$$P_{\mathcal{I}}(t_{or}) = \sum_i (1 - c(\tau_i - t_{or})^2) E_i. \quad (4.15)$$

The corresponding SINR is

$$\Gamma(t_{or}) = \frac{P_{\mathcal{S}}(t_{or})}{P_{\mathcal{I}}(t_{or}) + N_0/\sigma_x^2}. \quad (4.16)$$

4.4 Systems exploiting OFDM/DMT

OFDM is currently used for both wireless and wire-line communication networks, mainly under essentially identical schemes known as coded OFDM (COFDM) and discrete multi-tone modulation (DMT).

COFDM is an implementation of OFDM that includes coding for error detection and correction. DMT often refers to a baseband wire-line communication where the system adapts the transmission to the channel conditions individually for each sub-carrier. DMT is used for the asynchronous digital subscriber loop (ADSL).

The robustness of OFDM under multipath propagation has made it a strong candidate for future wireless standards. To date, most important contributions of OFDM are in Digital Audio Broadcasting (DAB), Digital Video Broadcasting (DVB), Integrated Services Digital Broadcasting (ISDB), Wireless LANs (WLAN), and Wireless MANs (WMAN).

In DVB, OFDM is considered for DVB-T (terrestrial) and DVB-H (handheld). In WLANs, OFDM is considered for IEEE 802.16 a and g systems, Hyper-LAN/2 and MMAC. More recently, OFDM has been also considered for 3G Long Term Evolution (LTE) mobile systems.

Chapter 5

Cooperative communication

It will be a core requirement of any future wireless communication systems to be able to support very high data rates. As this vision is not feasible with the conventional cellular architecture, in order to increase the capacity, different transmit diversity schemes have been thoroughly investigated over the past decade.

Cooperative communication is a method which enables different receivers in the network to share their antennas and generate a virtual multiple-antenna transmission in order to achieve transmit diversity. A relay station (RS) is a transceiver that forwards radio signals in the wireless network. It has been a main research topic as communication beyond third generation will have spectrum band above the 2 GHz where radio propagation is significantly more vulnerable to nonline-of-sight conditions. A solution would be to increase the BS density but the resulting high operator cost has motivated research into the use of relay transceivers to increase the number of network access points. Relays have many cost advantages and cost is the main argument for relay-based deployments [13]. Unlike the BSs, relays do not have to cover a large area which means that the transmit power requirements are significantly less critical than for the BSs. Furthermore, relays do not have a wired connection to the backbone network, and the mast on which the relay is placed does not need to be as high as for a BS, reducing operating expenses and maintenance costs for the service provider [48]. The use of multihop transmission through relays in a existing cellular systems has been shown to improve the performance for a lower cost than increasing the density of base stations [60]. However, introducing relay nodes creates new problem such as amplification of the noise and interference power.

Literature has foreseen cooperative communication between users where the user terminal would be also a relay station, relaying a duplicate of the same signal through different paths creating spatial diversity. In the following parts of this chapter, the

different types of relaying concept will be introduced. Figure 5.1 depicts a simple cooperative communication scenario.

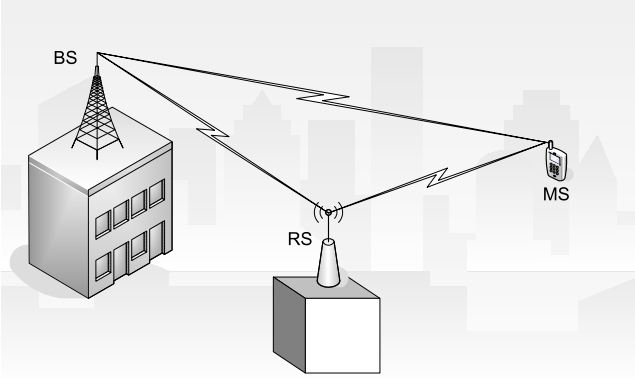

Figure 5.1: Simple cooperative communication

5.1 Basic relaying concepts

The expected benefits of different relay concepts are radio coverage extension and quality of service (QoS) enhancement. For this purpose different types of relays have been proposed as well as different types of transmission protocols to enhance the coverage, throughput and system capacity of the networks.

5.1.1 Relay station type

Relay stations have been discussed in, e.g., DVB-T/H and WiMAX (IEEE 802.16j) technical reports as a fixed, nomadic or mobile relay station.

- Fixed relay station (FRS): a relay station that is permanently installed at a fixed location.
- Nomadic relay station (NRS): a relay station that is intended to function from a location that is fixed for periods of time comparable to a user session.
- Mobile relay station (MRS): a relay station that is intended to function while in motion.

Meanwhile, this thesis will only consider the case of fixed relay stations introduced in a pre-established network.

5.1.2 Decode-and-forward and amplify-and-forward relaying

Depending on their nature and complexity, relays systems can be classified as either decode-and-forward (D&F) or amplify-and-forward (A&F) systems [26, 44]. D&F relaying, sometimes referred to as digital repeater, is more robust. It fully decodes the received signal from the first hop, and re-encodes and retransmits the decoded signal through the second hop. But the encoding and re-encoding process add non negligible delay. On the other hand, A&F relaying is a less complex system that just amplifies and forward the incoming signal without performing any forward error correction decoding and encoding. A&F relays have the advantage of introducing a minimum delay but have the drawback of amplifying the noise. Due to its simplicity, only A&F relaying will be consider in this thesis.

5.1.3 Full-duplex and half-duplex protocols

The broadcast nature of the wireless medium (usually seen as a drawback) can be exploited in cooperative relaying to achieve diversity with either the full-duplex or half-duplex protocol. In the full-duplex protocol, the relays receive and retransmit at the same time, so in full-duplex relaying, both, the signal from the BS and from the RS are received simultaneously. In half-duplex protocol the relays receive and

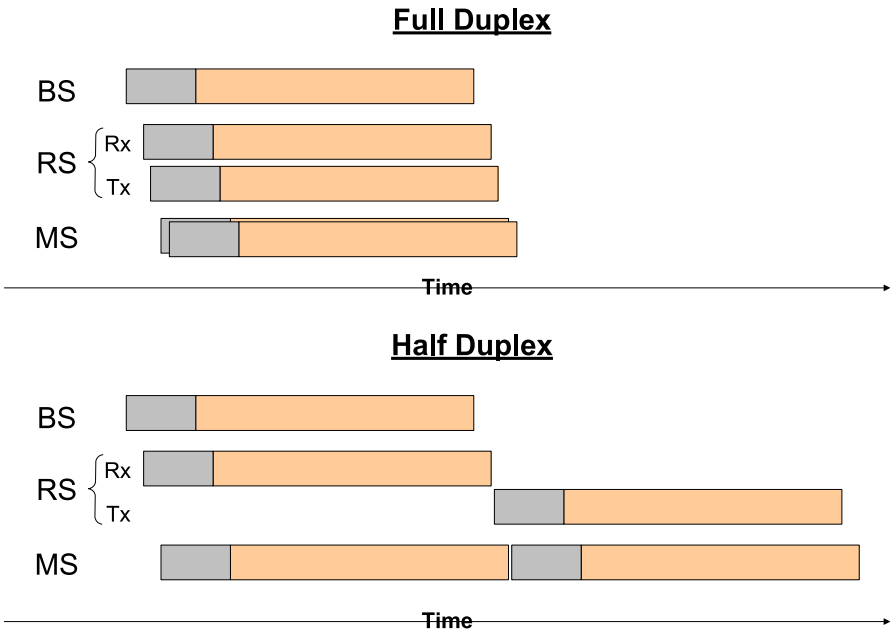

Figure 5.2: Full-duplex and half-duplex protocols

retransmit separately. In a first period of time only the BS sends the signal which is received by both the MS and the RS. In a second period of time, when the BS transmission is over, the relay forwards the signal. Unlike the full-duplex protocol, the half-duplex protocol allows different combining methods of the direct and relayed transmissions.

These two protocols are illustrated in Figure 5.2.

5.2 A&F relay channel model

We only consider downlink transmission as shown in Figure 5.3. The communication from the source (BS) to the destination (MS) goes through two links, the direct link and the relay link. The relay link is partitioned into two hops, the first hop is the link from the source to the relay and the second hop is the link from the relay to the source. We do not consider multi-hop transmission via several relays and we assume no interference from the relay itself [50].

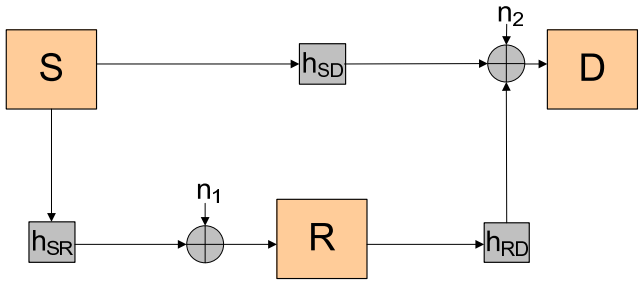

Figure 5.3: Relay channel model

The channel of the direct link is denoted h_{SD}. On the relay link, the RS received a noisy, attenuated version of the transmitted signal $s(t)$ after the first hop:

$$r_1(t) = h_{SR} * s(t) + n_1(t) \tag{5.1}$$

where '$*$' stands for convolution, h_{SR} is the channel of the first hop, and n_1 the noise at the relay receiver. The relay does not proceed to any processing and the signal is directly amplify by a factor β, and forward the following signal to the MS

$$\beta r_1(t) = \beta h_{SR} * s(t) + \beta n_1(t) \tag{5.2}$$

The overall channel of the relay link is thus $h_{SRD} = \beta h_{SR} * h_{RD}$. The processing

delay of the relay may be included in one of the channels h_{SR} or h_{RD}.

The notation $h_{XY}(\tau) = \sum h_i^{xy} \delta(\tau - \tau_i^{xy})$ is used to described a multipath channel on the 'XY' link . E_{XY} is the total channel energy and E_i^{xy} is the energy of the ith tap.

A&F relays can be classified into two subcategories, depending on their capability to perform and use channel state information (CSI). CSI-assisted relays use instantaneous CSI of the first hop to control the gain introduced by the relay in order to have a constant retransmitted signal power [26]. Ín contrast, relays which do not use instantaneous CSI, amplify the signal with a fixed gain which results in a variable power at the relay output. Although relays which are not CSI-assisted are not expected to perform as well as CSI-assisted relays, their low complexity and ease of deployment make them attractive from a practical point of view.

The most commons relay gains have been set for a flat fading channel. Next the three most common gains from the literature [53] are given with the following notation: σ_{bs}^2 and σ_{rn}^2 are the average transmit power for the BS and the RS respectively.

Fixed gain

The relay does not use any channel state information, it forwards the incoming signal with a fixed gain which guarantee a constant transmit power. The amplify-and-forward gain factor is defined as:

$$\beta^{FG} = \sqrt{\frac{\sigma_{rn}^2}{\sigma_{bs}^2 E_{SR} + N_0}} \tag{5.3}$$

Unlimited gain

The relay inverts the channel impulse response regardless of its magnitude, therefore if the channel is nearly null the relay may require an infinite gain which makes this gain not feasible.

$$\beta^{UG} = \sqrt{\frac{\sigma_{rn}^2}{\sigma_{bs}^2 \mid h_{SR} \mid^2}} \tag{5.4}$$

Variable gain

For this last gain, the channel state information must be available. The relays use this knowledge to equalize the fluctuation of the amplitude of the first hop channel.

$$\beta^{VG} = \sqrt{\frac{\sigma_{rn}^2}{\sigma_{bs}^2 \mid h_{SR} \mid^2 + N_0}} \tag{5.5}$$

The fixed gain and variable gain are two well-known relaying strategies. Fixed gain increases more the noise level but is easier to implement as it does not require CSI. The unlimited gain may require an infinite gain and transmitted power that are not feasible in practice but the resulting theoretical performance for this ideal gain is used as a benchmark for practical protocols.

5.3 Performance with full-duplex protocol

We now consider an OFDM transmission as described in Chapter 4. With the full-duplex protocol, the received signal from the source and the relay are directly combined:

$$\begin{aligned} r_2(t) &= h_{SD} * s(t) + \beta h_{RD} * r_1(t) + n_2(t) && (5.6)\\ &= (h_{SD} + h_{SRD}) * s(t) \; + \; \beta h_{RD} * n_1(t) + n_2(t) && (5.7)\\ &= h_{eq} * s(t) + n_{eq}(t) && (5.8) \end{aligned}$$

where h_{eq} is the overall equivalent channel attenuation

$$h_{eq}(\tau) = h_{SD}(\tau) + h_{SRD}(\tau) \tag{5.9}$$

and n_{eq} is the total equivalent noise which include the noise amplification due to the relay

$$n_{eq}(t) = \beta h_{RD} * n_1(t) + n_2(t). \tag{5.10}$$

For an OFDM signal, assuming the same noise power N_0 at the relay and the destination, the instantaneous SINR after demodulation of the block $i = 0$ is

$$\gamma_{FD}(n) = \frac{|\mathcal{H}_{n,n,0}^{eq}|^2}{\sum\limits_{\substack{l=0\\l\neq n}}^{N-1} |\mathcal{H}_{l,n,0}^{eq}|^2 + \sum\limits_{\substack{i=-\infty\\i\neq 0}}^{+\infty} \sum\limits_{l=0}^{N-1} |\mathcal{H}_{l,n,i}^{eq}|^2 + \left(\sum\limits_{j} |\beta h_j^{rd}|^2 + 1 \right) N_0/\sigma_x^2}. \tag{5.11}$$

where $\mathcal{H}_{l,n,i}^{eq}$ denotes the equivalent channel component at the nth DFT output caused by the symbol transmitted on the lth carrier during the ith block.

The corresponding average SINR for an OFDM system as describe in Equation 4.13 is

$$\Gamma_{FD} = \frac{P_{\mathcal{S}_{FD}}}{P_{\mathcal{I}_{FD}} + P_{\mathcal{N}_{FD}}/\sigma_x^2}. \tag{5.12}$$

where

$$P_{\mathcal{S}_{FD}} = \sum_i c(\tau_i^{eq})^2 E_i^{eq} \tag{5.13}$$

$$P_{\mathcal{I}_{FD}} = \sum_i (1 - c(\tau_i^{eq})^2) E_i^{eq} \tag{5.14}$$

$$P_{\mathcal{N}_{FD}} = \left(\mathcal{E}\left[|\beta|^2\right] E_{RD} + 1\right) N_0 \tag{5.15}$$

The average power E_i^{eq} and the expectation $\mathcal{E}\left[|\beta|^2\right]$ may be calculated by direct integration according to the channel and relay gain statistics. Fixed gain and variable gain relaying will have a different impact on the SINR. As relay gains have been only defined for a flat channel, we will assume h_{SR} flat but h_{RD} frequency selective. Assuming that the relay does not have any CSI of the second hop and the two hops are independent, we have

$$E_i^{eq} = \mathcal{E}\left[|h_{SD}(\tau_i^{eq})|^2\right] + \mathcal{E}\left[|h_{RD}(\tau_i^{eq})|^2\right] \mathcal{E}\left[|\, \beta h_{SR}\,|^2\,\right]. \tag{5.16}$$

We finally see that every paths of h_{RD} is multiplied by the same power. We then derive the two useful expectations, $\mathcal{E}\left[|\, \beta h_{SR}\,|^2\,\right]$ and $\mathcal{E}\left[|\beta|^2\right]$, for the fixed and variable gain respectively.

Fixed gain

The fixed relay gain depends only of the average energy of the channel: $\beta^{FG} = \sqrt{\frac{\sigma_{rn}^2}{\sigma_{bs}^2 E_{SR} + \sigma_n^2}}$, where σ_{bs}^2 and σ_{rn}^2 are the average transmit power for the BS and the RS respectively. So, the relay amplifies the signal power by

$$\mathcal{E}\left[|\, \beta^{FG} h_{SR}\,|^2\right] = |\beta^{FG}|^2 \mathcal{E}\left[|\, h_{SR}\,|^2\right] = \frac{\sigma_{rn}^2 E_{SR}}{\sigma_{bs}^2 E_{SR} + N_0}, \tag{5.17}$$

and the relay amplifies the noise by

$$\mathcal{E}\left[\mid \beta^{FG} \mid^2\right] = \frac{\sigma_{rn}^2}{\sigma_{bs}^2 E_{SR} + N_0}. \tag{5.18}$$

Variable gain

The variable relay gain fluctuates as a function of the instantatenous fading of the first hop: $\beta^{VG} = \sqrt{\frac{\sigma_{rn}^2}{\sigma_{bs}^2 |h_{SR}|^2 + N_0}}$. The relay amplifies the useful power by

$$\mathcal{E}\left[\mid \beta^{VG} h_{SR} \mid^2\right] = \mathcal{E}\left[\frac{\sigma_{rn}^2 \mid h_{SR} \mid^2}{\sigma_{bs}^2 \mid h_{SR} \mid^2 + N_0}\right] \tag{5.19}$$

which can be derived for the general Nakagami fading where the power of the link is Gamma distributed such that

$$\mid h_{SR} \mid^2 \sim \mathcal{G}(x, m, \frac{E_{SR}}{m}) = \frac{x^{m-1}}{(\frac{E_{SR}}{m})^m \Gamma(m)} e^{\frac{-mx}{E_{SR}}} = \frac{m^m}{E_{SR}^m \Gamma(m)} x^{m-1} e^{\frac{-mx}{E_{SR}}}. \tag{5.20}$$

Therefore,

$$\mathcal{E}\left[\mid \beta^{VG} h_{SR} \mid^2\right] = \frac{m^m}{E_{SR}^m \Gamma(m)} \int_0^\infty \frac{\sigma_{rn}^2 x^m}{\sigma_{bs}^2 x + N_0} e^{-\frac{mx}{E_{SR}}} \mathrm{d}x \tag{5.21}$$

$$\mathcal{E}\left[\mid \beta^{VG} h_{SR} \mid^2\right] = \frac{\sigma_{rn}^2 m}{\sigma_{bs}^2} \; e^{\frac{mN_0}{E_{SR}\sigma_{bs}^2}} \; \mathrm{E}_{m+1}\left(\frac{m\, N_0}{E_{SR}\sigma_{bs}^2}\right). \tag{5.22}$$

The exponential integral can be express in term of the incomplete gamma function:

$$\mathrm{E}_n(x) = x^{n-1}\, \Gamma\left(1-n, x\right) \tag{5.23}$$

$$\mathcal{E}\left[\mid \beta^{VG} h_{SR} \mid^2\right] = \frac{\sigma_{rn}^2 m}{\sigma_{bs}^2} \; e^{\frac{mN_0}{E_{SR}\sigma_{bs}^2}} \; \left(\frac{mN_0}{E_{SR}\sigma_{bs}^2}\right)^m \; \Gamma\left(-m, \frac{mN_0}{E_{SR}\sigma_{bs}^2}\right). \tag{5.24}$$

The relay amplifies the noise by

$$\mathcal{E}\left[\mid \beta^{VG} \mid^2\right] = \mathcal{E}\left\{\frac{\sigma_{rn}^2}{\sigma_{bs}^2 \mid h_{SR} \mid^2 + N_0}\right\}. \tag{5.25}$$

Where both results are given using in term of the exponential integral function or

incomplete gamma function:

$$\mathcal{E}\left[\mid \beta^{VG} \mid^2\right] = \frac{\sigma_{rn}^2 m}{E_{SR}\sigma_{bs}^2}\, e^{\frac{mN_0}{E_{SR}\sigma_{bs}^2}}\, \mathrm{E}_m\left(\frac{m\,N_0}{E_{SR}\sigma_{bs}^2}\right) \tag{5.26}$$

$$\mathcal{E}\left[\mid \beta^{VG} \mid^2\right] = \frac{\sigma_{rn}^2 m}{E_{SR}\sigma_{bs}^2}\, e^{\frac{mN_0}{E_{SR}\sigma_{bs}^2}}\, \left(\frac{mN_0}{E_{SR}\sigma_{bs}^2}\right)^m \Gamma\left(1-m, \frac{m\,N_0}{E_{SR}\sigma_{bs}^2}\right).d \tag{5.27}$$

5.4 Performance with half-duplex protocol

The half-duplex protocol allows us to apply different combining strategies. In an OFDM system, different combining methods can be applied before or after the DFT, and hence called pre-DFT combining or post-DFT combining [45]. We will only consider post-DFT combining, we assume that the receiver is able to estimated the instantaneous SINR on the nth subcarrier $\gamma(n)$ as in Equation (4.13). On the nth subcarrier, after demodulation, we have the two receive signals

$$y_{SD}[n] = x_{0,n}\mathcal{H}_{n,n,0}^{sd} + \sum_{\substack{l=0\\ l\neq n}}^{N-1} x_{0,l}\mathcal{H}_{l,n,0}^{sd} + \sum_{\substack{i=-\infty\\ i\neq 0}}^{+\infty}\sum_{l=0}^{N-1} x_{i,l}\mathcal{H}_{l,n,i}^{sd} + \tilde{n}_{SD}[n] \tag{5.28}$$

$$y_{SRD}[n] = x_{0,n}\mathcal{H}_{n,n,0}^{srd} + \sum_{\substack{l=0\\ l\neq n}}^{N-1} x_{0,l}\mathcal{H}_{l,n,0}^{srd} + \sum_{\substack{i=-\infty\\ i\neq 0}}^{+\infty}\sum_{l=0}^{N-1} x_{i,l}\mathcal{H}_{l,n,i}^{srd} + \tilde{n}_{SRD}[n] \tag{5.29}$$

with the corresponding instantaneous SINR and average SINR $\gamma_{SD}(n)$, $\gamma_{SRD}(n)$, Γ_{SD} and Γ_{SRD}, respectively.

Next, are reviewed the most common combining methods known as selection, equal gain and maximum ratio combining.

5.4.1 Selection combining

The receiver chooses to select only the received signal with the best SINR as follows,

$$y_{HD-SC}[n] = \arg \max_{y_{XY}[n]\in\{y_{SD}[n], y_{SRD}[n]\}} \gamma_{XY}(n) \tag{5.30}$$

thus

$$\gamma_{HD-SC}(n) = \max(\gamma_{SD}(n), \gamma_{SRD}(n)). \tag{5.31}$$

We are not able to compute the average SINR of this scheme, Γ_{HD-SC}, but we have the straightforward lower bound:

$$\Gamma_{HD-SC} \geq \max(\Gamma_{SD}, \Gamma_{SRD}). \tag{5.32}$$

This bound will be achieved if the receiver does not choose the best instantaneous link but the best link on average.

5.4.2 Equal gain combining

The receiver sums each received signal after a co-phased operation.

$$y_{HD-EGC}[n] = e^{-j\theta_{sd}} y_{SD}[n] + e^{-j\theta_{srd}} y_{SRD}[n] \tag{5.33}$$

where $\theta_{sd} = \angle \mathcal{H}^{sd}_{n,n,0}$ and $\theta_{srd} = \angle \mathcal{H}^{srd}_{n,n,0}$.

The resulting instantaneous SINR is

$$\gamma_{HD-EGC}(n) = \frac{\mathcal{S}_{HD-EGC}(n)}{\mathcal{I}_{HD-EGC}(n) + \mathcal{N}_{HD-EGC}/\sigma_x^2}. \tag{5.34}$$

with

$$\mathcal{S}_{HD-EGC}(n) = \left(|\mathcal{H}^{sd}_{n,n,0}| + |\mathcal{H}^{srd}_{n,n,0}|\right)^2 \tag{5.35}$$

$$\mathcal{I}_{HD-EGC}(n) = \sum_{\substack{l=0 \\ l\neq n}}^{N-1} |\mathcal{H}^{sd}_{l,n,0} e^{-j\theta_{sd}} + \mathcal{H}^{srd}_{l,n,0} e^{-j\theta_{srd}}|^2 \tag{5.36}$$

$$+ \sum_{\substack{i=-\infty \\ i\neq 0}}^{+\infty} \sum_{l=0}^{N-1} |\mathcal{H}^{sd}_{l,n,i} e^{-j\theta_{sd}} + \mathcal{H}^{srd}_{l,n,i} e^{-j\theta_{srd}}|^2 \tag{5.37}$$

$$\mathcal{N}_{HD-EGC} = \left(\sum_j |\beta h_j^{rd}|^2 + 2\right) N_0. \tag{5.38}$$

Assuming that the channels on the relay and direct link are independent, the corresponding average SINR, Γ_{HD-EGC} is

$$\Gamma_{HD-EGC} = \frac{P_{\mathcal{S}_{HD-EGC}}}{P_{\mathcal{I}_{HD-EGC}} + P_{\mathcal{N}_{HD-EGC}}/\sigma_x^2} \tag{5.39}$$

where

$$P_{\mathcal{S}_{HD-EGC}} = \sum_i c(\tau_i^{eq})^2 E_i^{eq} + 2\mathcal{E}\left[|\mathcal{H}_{n,n,0}^{sd}|\right]\mathcal{E}\left[|\mathcal{H}_{n,n,0}^{srd}|\right] \quad (5.40)$$

$$P_{\mathcal{I}_{HD-EGC}} = \sum_i (1 - c(\tau_i^{eq})^2) E_i^{eq} \quad (5.41)$$

$$P_{\mathcal{N}_{HD-EGC}} = \left(\mathcal{E}\left[|\beta|^2\right] E_{RD} + 2\right) N_0. \quad (5.42)$$

Furthermore, if we assumed as well the channel taps of h_{SD} distributed such as $h_i^{sd} \sim \mathcal{CN}(0, E_i^{sd})$; since

$$\mathcal{H}_{n,n,0}^{sd} = \sum_i c(iT) h_{SD}(iT) e^{-j\frac{2\pi ni}{N}}$$

is the sum of independent Gaussian variables, we have

$$\mathcal{H}_{n,n,0}^{sd} \sim \mathcal{CN}(0, \sum_i c(\tau_i^{sd})^2 E_i^{sd}).$$

As a consequence, its norm is Rayleigh distributed

$$|\mathcal{H}_{n,n,0}^{sd}| \sim \text{Rayleigh}\left(\sqrt{\frac{1}{2}\sum_i c(\tau_i^{sd})^2 E_i^{sd}}\right)$$

with a mean of

$$\mathcal{E}\left[|\mathcal{H}_{n,n,0}^{sd}|\right] = \sqrt{\frac{\pi}{4}\sum_i c(\tau_i^{sd})^2 E_i^{sd}}.$$

In order to evaluate $\mathcal{E}\left[|\mathcal{H}_{n,n,0}^{srd}|\right]$, we will assume that the first hop of the relay link is a single tap channel, we may then write

$$\mathcal{H}_{n,n,0}^{srd} = \sum_i c(iT) h_{SRD}(iT) e^{-j\frac{2\pi ni}{N}} = \beta h_{SR} \sum_i c(iT) h_{RD}(iT) e^{-j\frac{2\pi ni}{N}}.$$

Accordingly, its expectation simplied to

$$\mathcal{E}\left[|\mathcal{H}_{n,n,0}^{srd}|\right] = \mathcal{E}\left[|\beta h_{SR}|\right]\mathcal{E}\left[|\mathcal{H}_{n,n,0}^{rd}|\right].$$

In the same manner if h_{SR} and the taps of h_{RD} are complex Gaussian, we may show that

$$\mathcal{E}\left[|\mathcal{H}_{n,n,0}^{rd}|\right] = \sqrt{\frac{\pi}{4}\sum_i c(\tau_i^{rd})^2 E_i^{rd}}$$

and

$$\mathcal{E}\left[|\beta h_{SR}|\right] = \sqrt{\frac{\pi}{4}\beta E_{SR}}$$

with fixed relay gain. Combining these results, we have

$$\mathcal{E}\left[|\mathcal{H}^{srd}_{n,n,0}|\right] = \frac{\pi}{4}\sqrt{\beta^2 E_{SR}\left(\sum_i c(\tau_i^{rd})^2 E_i^{rd}\right)} = \frac{\pi}{4}\sqrt{\sum_i c(\tau_i^{srd})^2 E_i^{srd}}.$$

Finally, with the assumptions stated above, the average useful power is equal to

$$P_{\mathcal{S}_{HD-EGC}} = \sum_i c(\tau_i^{eq})^2 E_i^{eq} + 2\left(\frac{\pi}{4}\right)^{3/2}\sqrt{\sum_i c(\tau_i^{sd})^2 E_i^{sd}}\sqrt{\sum_i c(\tau_i^{srd})^2 E_i^{srd}}. \quad (5.43)$$

5.4.3 Maximum ratio combining

The optimum combining scheme in terms of instantaneous SINR is given by maximum ratio combining. All received signals are co-phased and scaled as follows

$$y_{HD-MRC}[n] = \frac{\left(\mathcal{H}^{sd}_{n,n,0}\right)^*}{\mathcal{I}_{SD}(n) + N_0/\sigma_x^2} y_{SD}[n] \quad + \frac{\left(\mathcal{H}^{srd}_{n,n,0}\right)^*}{\mathcal{I}_{SRD}(n) + \mathcal{N}_{SRD}/\sigma_x^2} y_{SRD}[n]. \quad (5.44)$$

The resulting instantaneous SINR is

$$\gamma_{HD-MRC}(n) = \frac{\mathcal{S}_{HD-MRC}(n)}{\mathcal{I}_{HD-MRC}(n) + \mathcal{N}_{HD-MRC}/\sigma_x^2} \quad (5.45)$$

with

$$\begin{aligned}
\mathcal{S}_{HD-MRC}(n) &= \left(\gamma_{SD}(n) + \gamma_{SRD}(n)\right)^2 && (5.46)\\
\mathcal{I}_{HD-MRCC}(n) &= \sum_{\substack{l=0\\ l\neq n}}^{N-1}\left|\frac{\mathcal{H}^{sd}_{l,n,0}\left(\mathcal{H}^{sd}_{n,n,0}\right)^*}{\mathcal{I}_{SD}(n) + N_0/\sigma_x^2} + \frac{\mathcal{H}^{srd}_{l,n,0}\left(\mathcal{H}^{srd}_{n,n,0}\right)^*}{\mathcal{I}_{SRD}(n) + \mathcal{N}_{SRD}/\sigma_x^2}\right|^2 && (5.47)\\
&\quad + \sum_{\substack{i=-\infty\\ i\neq 0}}^{+\infty}\left|\frac{\mathcal{H}^{sd}_{l,n,i}\left(\mathcal{H}^{sd}_{n,n,0}\right)^*}{\mathcal{I}_{SD}(n) + N_0/\sigma_x^2} + \frac{\mathcal{H}^{srd}_{l,n,i}\left(\mathcal{H}^{srd}_{n,n,0}\right)^*}{\mathcal{I}_{SRD}(n) + \mathcal{N}_{SRD}/\sigma_x^2}\right|^2 && (5.48)\\
\mathcal{N}_{HD-MRC} &= \frac{N_0}{|\mathcal{I}_{SD}(n) + N_0/\sigma_x^2|^2} + \frac{\mathcal{N}_{SRD}}{|\mathcal{I}_{SRD}(n) + \mathcal{N}_{SRD}|^2}. && (5.49)
\end{aligned}$$

Unfortunately, we are not able to derive the average SINR of this combining scheme.

Chapter 6

Simulator development

In order to evaluate the performance of different relaying concepts for DVB-H/T and MBMS in 3G, a simulator was built. The air interface is OFDM and most of the simulation parameters have been selected from 3G long-term evolution (LTE). The chosen performance metric is the average SINR for an OFDM system described as in Chapter 4. This chapter describes the network architecture, the simulation scenario, parameters and variables.

6.1 Network architecture

The network is a cellular, single frequency network.

6.1.1 Cellular network

The radio network is modeled as a cellular network. The set of BSs is assumed to form a hexagonal lattice meaning that a single BS has six closest neighbors at equal distances from each other. The inter-site distance (ISD) which is the distance from one BS to its closest neighbor is a parameter in the program. The total area is divided into sub-areas called cells each cell being mainly covered by a single BS. We assume that the network is the superposition of cells tiers around a central cell. It is easy to see that the first tier has 6 cells, the second tier has 12, and the nth tier comprises $6n$ cells. The total number of cells is thus $1 + 3N_{tier}(N_{tier} + 1)$ where N_{tier} is the total number of tiers around the central cell. We are interested in two types of cells, a simple hexagonal cell and a "sectorized" cell where each sector has a hexagonal shape. The Figure 6.1 is an example of this two network topologies with one tier of cells around the central cell.

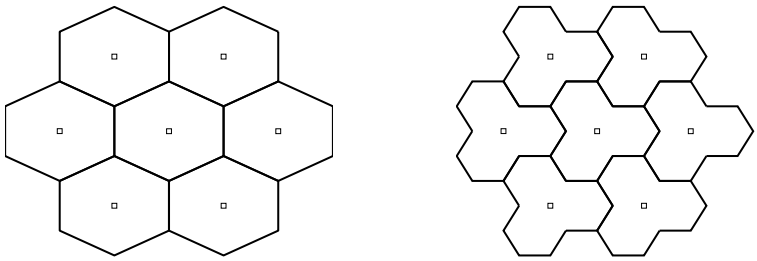

(a) Hexagonal cell (b) 3 sectors cell

Figure 6.1: Cellular network

6.1.2 Single frequency network

A single frequency network (SFN) is a broadcast network where transmitters send the same signal through the same radio resources aiming an efficient utilization of the spectrum. This type of network is exploited, e.g., for the standardization of MBMS (Multimedia Broadcast Multicast Service) in 3GPP. As the receiver will receive multiple signals from all the transmitters, an SFN transmission increases the time dispersion phenomenon. The time dispersion is then the mixture of the initial dispersion of each BS-MS links, and dispersion due to the reception of signals from several transmitters placed at different distances from the receiver. For an OFDM system, while superposition of multiple signals will increase the received signal power, the resulting long delay spread will increase the interferences. In order to enhance the performance, the transmitters are usually synchronized among each other.

6.2 Simulation scenario

Downlink OFDM-based transmission is considered. The network is composed of base stations, possibly relays, and one mobile station which is roaming in the central cell. The shape of the cells can be chosen as describe above. The MS is placed randomly in the central cell 10000 times; its location is uniformly distributed over the area. Figure 6.2 shows an example of a simulation for 5000 times with a sectorized cell. At each location the average SINR as described in Chapter 4 are computed. The distances from the MS to every transmitter is computed in order to calculate the path loss and the median of the delay spread according to the distance. We do not consider fast fading but, for every iteration, a different shadowing and

RMS delay spread is randomly generated. The results are presented as a cumulative distribution function of the SINR values. The SINR is different depending on the location of the MS in the cell.

Some simulations have also been run to simulate the result at the border of two SFNs. For this, we have considered that the central cell is at the border of another SFN meaning that all the signal from half of the BSs are thus entirely regarded as interferences. Later, fixed relays have been added. When considering relay transmission, we have assumed that the relay only forwards the signal from its serving BS, we have thus neglected the signal from other cells and the self interference from the relay itself. These assumptions can be physically justified if the relay is equipped with two different antennas, one for receiving and one for transmitting [49, 51]. As the relay is fixed, it may be assumed that the receive antenna is directed to its cell's BS.

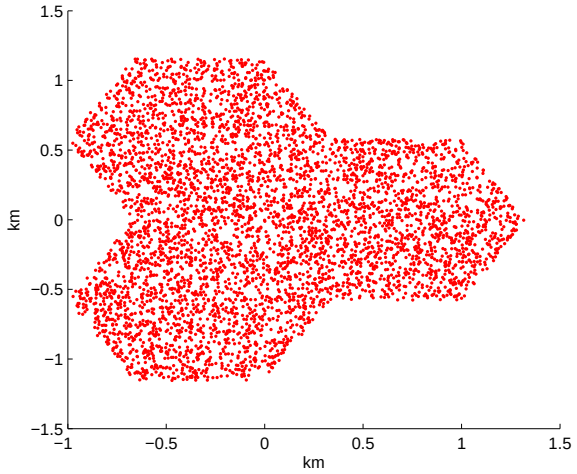

Figure 6.2: 5000 random locations of the MS

6.3 Simulation parameters

Most of the simulation parameters have been selected from 3G long-term evolution (LTE) [1, 2, 23].

6.3.1 OFDM parameters

The parameters are outlined below, taken from [1]. For all the simulations these parameters are unchanged, we have concentrated on the 10 MHz bandwidth option and the corresponding parameters. The bandwidth is 10 MHz with the center frequency at 2 GHz, the number of subcarriers in the OFDM frame is 1024 but only 601 are considered occupied. The length of the cyclic prefix is chosen as 16.67μs. The sampling frequency is at 15.36 MHz, the CP is thus of length 256.

Time of reference

As discussed in Chapter 4, the average SINR is a variable of the time of reference, which is the starting demodulation (FFT) time at the receiver. In order to maximize the useful signal power, it is important to synchronize the bias function with the time delay profile in such a way that most of the channel energy lies within the CP interval of the bias function. We have implemented three simple algorithms:

- *"Zero" method.* The MS is only synchronized with its own base station.
- *"First" method.* The receiver starts to demodulate the signal since the first received path.
- *"Max" method.* The receiver starts to demodulated the signal at the maximum power path.

The "First" method positions the time delay profile at the beginning of the CP interval of the bias function. The SINR is calculated at this position keeping in mind that the signal from the closest BS is also the signal with the highest power reaching the receiver and hence contains most of the channel energy.

However, as this method does not have the capacity to adjust to any unexpected changes, especially in cases of longer distances being involved, we have implemented the "Max" method. This method shifts the bias function over the power delay profile to have its initial time at the maximum power received path. The idea behind this method is to assume that most of the power is concentrated around the strongest path and avoids the loss of useful power if most of the delays are rather long.

These two methods have few complexities to implement while they provide good results as can be seen in the comparison of Figure 6.3. As shown in Figure 6.3(b), the "First" method gives the best result. Figure 6.3(a) exemplifies when the bias function of the "First" method is placed in such a way that the CP interval contains most of the channel energy. According to this result, all the next simulation will be performed with the "First" method.

Finally, we note that an optimum method would have been to shift the bias function over the power delay profile and determine the best position yielding to the maximum SINR. This adaptive method always finds the best possible SINR by positioning the bias function. However, the method is time consuming since it needs to shift over all taps to calculate and compare for the maximum useful signal power.

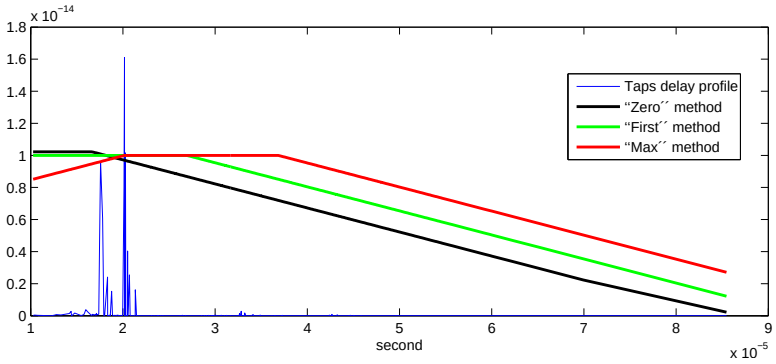

(a) A power delay profile versus the bias functions

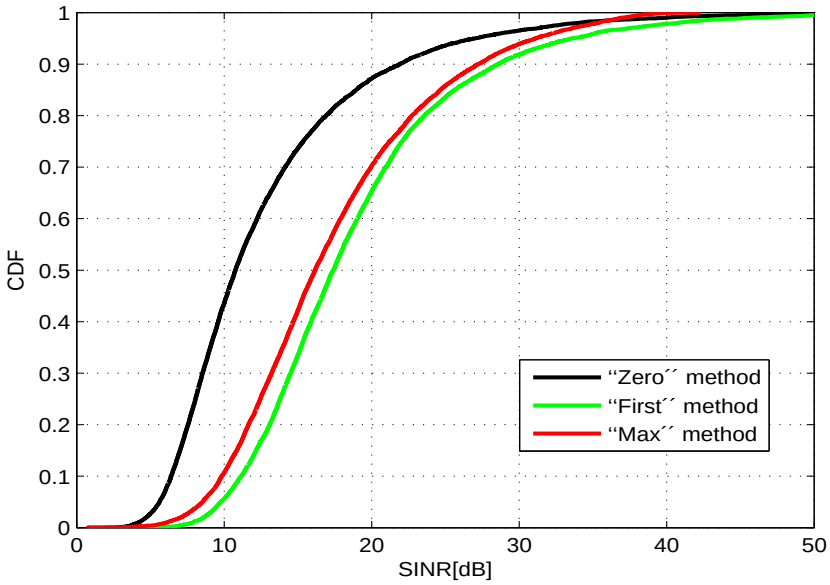

(b) Empirical CDF of the SINR

Figure 6.3: Comparaison between the different TOR algorithms

6.3.2 Network parameters

The number of tiers around the central cell has been chosen equal to five. Figure 6.4 shows that adding a tier of cells decreases the performance of the SFN as it increases the amount of interference (considering no interfering neighbor network). The performance is quite similar from 5 to 7 tiers, in order to avoid too long computation time we have chosen 5 tiers of cells around the central cell which means 91 cells in total.

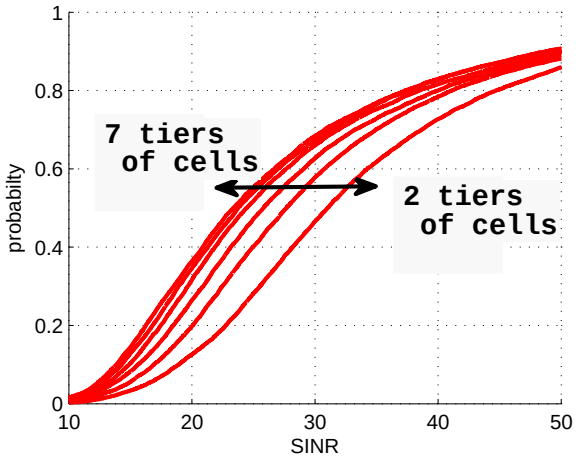

Figure 6.4: CDF of the SINR for different number of tiers

The cell synchronization is a parameter of the network. The cell synchronizations are the time offsets among the base stations. The time offset is taken from a time interval with a uniform distribution. The bound of this interval is chosen between 0, 10 and 20 seconds. When considering relay transmission, an additional processing delay of 0.5μs has been chosen.

The inter site distance (ISD) is the distance from a BS to its closest neighbor. The ISD is identical for all the BSs. The different chosen values are 2, 5, and 10 km. For a sectorized cell, a cell is composed of three hexagonal sectors of radius $R_s = \frac{ISD}{3}$.

6.3.3 Transmit power, antenna gain and antenna pattern

The average transmit power and antenna gain of the BS is chosen to 46 dBm and 14 dBi respectively. This gives a total beam power of 60 dBm, this value is often chosen as it is in accordance with the Federal Communications Commissions (USA)

which fixes the limit at 62.0 dBm minus a 1.5 dBm margin. Two types of antenna pattern have been implemented: an omnidirectional antenna which radiates power uniformly in the transmission plane, and a three sectorized antenna. Figure 6.5 shows the antenna pattern of the sectorized antenna.

The relay transmit power has been chosen equal to 37 dBm with an overall antenna gain of 12 dBi. The relay antenna pattern is chosen omnidirectional. These values are taken according to the literature, see for example [34, 64].

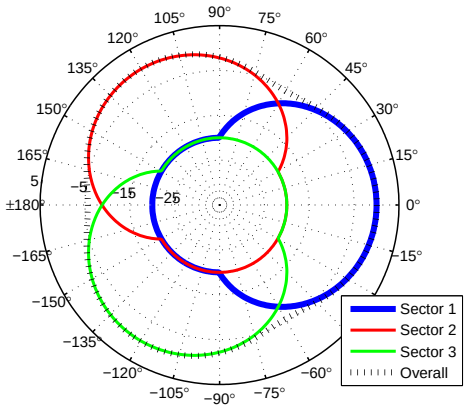

Figure 6.5: Three sectors antenna pattern

6.3.4 Channel models

Three different transmission links can be considered. The BS-MS and RS-MS links have been considered identical but the BS-RS link is different as a fixed relay should benefit from a good location regarding its BS. Both the BS-MS and RS-MS links are considered to be Rayleigh multipath channels, more specifically a type of channel called 6 typical urban (6TU) which is specified in the table below. The BS-RS link is considered as a flat Rayleigh channel.

6TU channel	1	2	3	4	5	6
Normalized relative delay	0.00	0.04	0.12	0.32	0.48	1.00
Normalized relative power	0.189	0.379	0.239	0.095	0.060	0.038

At every iteration, a different shadowing component and RMS delay spread are calculated as correlated lognormal variables. The RMS delay spread is calculated

according to Equation (2.6), with a median value of 0.65 μs and an exponent of 0.5. The standard deviation of the delay spread is chosen as 2 dB. From the RMS delay spread the channel taps delay are calculated using the 6TU table and Equation (2.5). In the same manner the tap energy are computed from the generated lognormal component, the 6TU table and Equation (2.4). The shadowing deviation has been chosen equal to 8 dB for the BS-MS and RS-MS links, and equal to 4 dB for the BS-RS link.

For the initial SFN simulation without relay the path loss model was chosen according to [1]. We have then used the more general model from IEEE 802.16 which takes into account the height of the transmitters and receivers in order to more realistically model the benefit of relaying. The BS, RS and MS heights have been chosen equal to 32, 12 and 1.5 respectively. The first hop of the relay is assumed to be line of sight and does not suffer from interference. The second hop of the relay link and the direct link are assumed to transmit under NLOS channel conditions. The different path losses are plotted in Figure 6.6. It is assumed that there are no loopback interferences and interfering signals from a relay output to another relay's input. These interferences may be avoided by, e.g. placing receive antennas on rooftops and transmit antennas at the street level, using highly directive receive antennas at relays and employing interference cancellation algorithms [52].

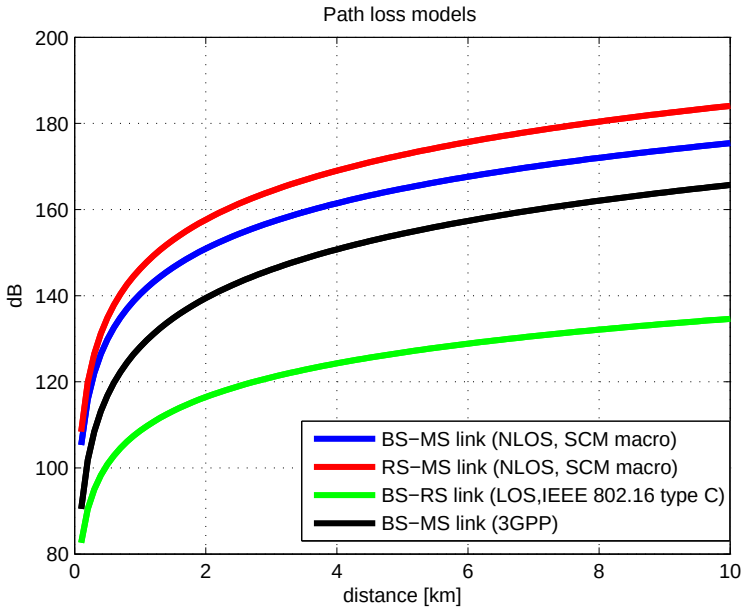

Figure 6.6: Path loss models

We have also implemented different correlation models among the large scale parameters (LSP) as presented in Chapter 3. Figure 6.7 shows the CDF of the SINR for different models:

- no correlation among the LSP
- correlation between the delay spread and shadowing of the same link is equal to $\rho_{XY} = -0.75$, no other correlations are considered
- cross-correlated shadowing between two links are equal to 0.5, the correlation between the delay spread and shadowing of the same link is changed to $\rho_{XY} = -0.6$ in order to end up with a positive definite matrix
- cross-correlation between two links are calculated according to the "Graziosi" model, the correlation between the delay spread and shadowing of the same link is $\rho_{XY} = -0.6$, the overall correlation matrix is calculated with a Kronecker product as explained at the end of Chapter 3
- cross-correlation between two links are calculated according to the "Saunders" model, the correlation between the delay spread and shadowing of the same link is $\rho_{XY} = -0.6$, the overall correlation matrix is also calculated with a Kronecker product.

In this figure, we see that most of those models almost do not have an impact on the SINR distribution. As there are no well-agreed models, we have just kept the correlation between the RMS delay spread and the shadowing of the same link equal to -0.75 and omitted any other correlations.

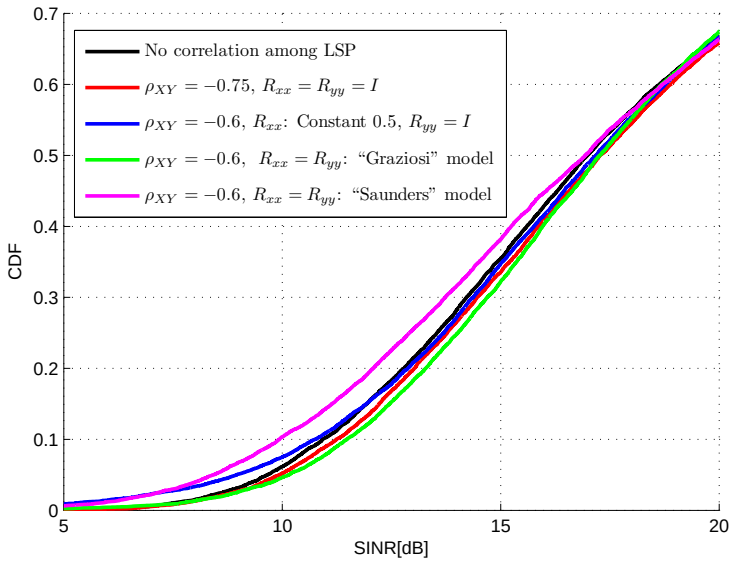

Figure 6.7: SINR with different correlation models

6.4 Summary tables

The following tables show the simulation parameters used if not stated otherwise are given; if a parameter is modified for a simulation it would then be mentioned.

Network topology	5 tiers cellular network
Bandwidth	10 MHz
Center frequency	2 GHZ
Number of subcarrier	1024
Number of occupied subcarrier	601
Propagation	$L = 128.1 + 37.6 * \log_{10}(R)$ 8 dB shadowing
Tx Power	46 dBm
BS antenna gain	14 dBi
Noise factor	9dB
Channel model	6 tap TU channel model Modelling of the delay spread: [33]
Cell synchronization	0 and 20μs
CP	16.67μs
ISD	2, 5 and 10 km
ISI and ICI modeling	According to [59]

Table 6.1: Simulation parameters for SFN without relays

Parameter	**Assumption**
Network	5 tiers tri-sector cell
ISD	2 km
Bandwidth	10 MHz
Center frequency	2 GHz
Number of subcarrier	1024
Number of occupied subcarrier	601
Cell synchronization	$20\mu s$
CP	$16.67\mu s$
Relay processing delay	$0.5\mu s$
ISI and ICI modeling	According to [59]
Beam Tx power Relay Tx power	40 Watts / 46 dBm 5 Watts / 37 dBm
Antenna gain BS Antenna gain RS	14 dBi 12 dBi (in total for Rx and Tx)
Antenna pattern BS	3 sectors $A(\theta) = -min\left[12\left(\frac{\theta}{\theta_{3dB}}\right)^2, A_m\right]$ $\theta_{3dB} = 70°, \quad A_m = 20dB$
Antenna pattern RS	omnidirectional
Noise figure	9 dB
Thermal noise	-174 dBm/Hz
Pathloss BS-MS link and RS-MS link	(NLOS, SCM macro): $PL(dB) = (44.9 - 6.55\log_{10} h_{bs})\log_{10}(d[km])$ $+45.5 + (35.46 - 1.1h_{ms})\log_{10}(f_c[MHz])$ $+13.82\log_{10}(h_{bs}) + 0.7h_{ms} + 3$
Pathloss BS-RS link	(LOS,IEEE 802.16 type C): $PL(dB) = -35.4 + 26\log_{10}(d[m])$ $+20\log_{10}(f_c[MHz])$
Heights h_{bs}, h_{rs}, h_{ms}	$32, 12, 1.5$ meters
Shadowing standard deviation	8 dB standard deviation for BS-MS and RS-MS link 4 dB standard deviation for BS-RS link
Shadowing correlation	omitted
Channel model: BS-MS and RN-MS link BS-RN link	 6 taps TU channel model flat Rayleigh channel

Table 6.2: Simulation parameters for SFN with relays

Chapter 7

Simulation results

In this chapter different simulation results are presented. As a first step, an SFN without relay has been implemented and simulated. These first simulations were used as a benchmark to gauge the quality of the simulator with comparison to the results of [43]. Relays have then been introduced into the network and different relaying concepts have been evaluated as introduced in Chapter 5, as well as the impact of relay topology chosen among different numbers and repartitions.

7.1 SFN area deployment aspects

As a first step in the simulation work, this section reviews the result of [43] on SFN area deployment aspects. Different simulations have been run to assess the impact of inter-site distance (ISD), asynchronity, and other factors such as distance from the border of two SFNs and the effect of possible holes in the SFN grid. The asynchronity refers to the time offset an OFDM frame is sent among the BSs. In our model each BS in the network has a random offset which is uniformly distributed in the range $[0, Async]$, where the upper bound is the maximum time offset in the SFN. The simulation parameters used in this section are issued from Table 6.4.

7.1.1 Impact of asynchronity and ISD

From Figure 7.1, the SINR distribution is clearly dependent on the ISD value: the smaller the ISD is, the higher the SINR. One can notice also, that the synchronization of the BSs has a real impact in the low ISD case but not in the high ISD case. Being far from the sources reduces naturally the signal-to-noise ratio because the attenuation mainly increases with the distance. Interference suffers from the same attenuation as the useful signal so even if the proportion of the interfering signal is

more important with a high ISD, they are more attenuated and the noise becomes prominent. Introducing asynchronity has not a real impact in the low BSs density case, because the delay caused by asynchronity become negligible compared to the high physical delay due to the longer path, and also because the attenuation get higher with a high ISD.

In Figure 7.2, we see that at the border of two SFNs, asynchronity does not have any impact. At the border of two SFNs, the presence of interference is very high because half of the neighboring cells interfere. Also at the border, the effect of asynchronity is very slight, because in the interference proportion the level from the interfering SFN is already very high. In the middle of the SFN, the situation is the reverse, the interference level by another SFN is low and in general the SINR is relatively high, so the asynchronity effect gets higher. The SINR expression given by Equation (4.13) shows that a small delay outside the cyclic prefix decreases the useful signal by a power of two and at the same time increases the interference by a power of two.

In conclusion, asynchronity is not an important issue in the deployment aspect of an SFN, because asynchronity only deteriorates the SINR where it is already very high and the resulting SINR is still good, and on the other hand, asynchronity does not have any effect on the low SINR region.

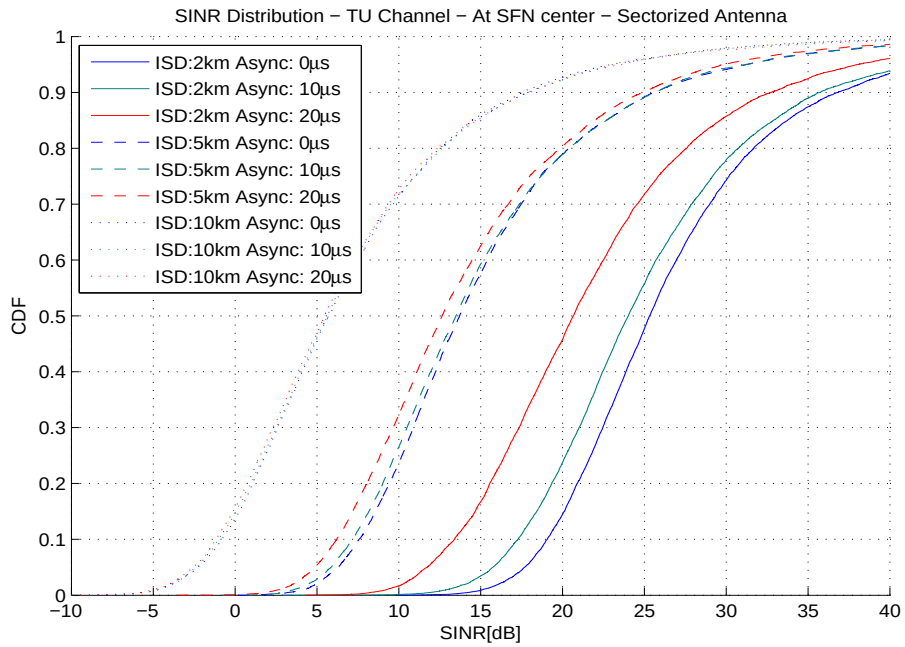

Figure 7.1: The impact of asynchronity and ISD on SINR distribution at the center of the SFN

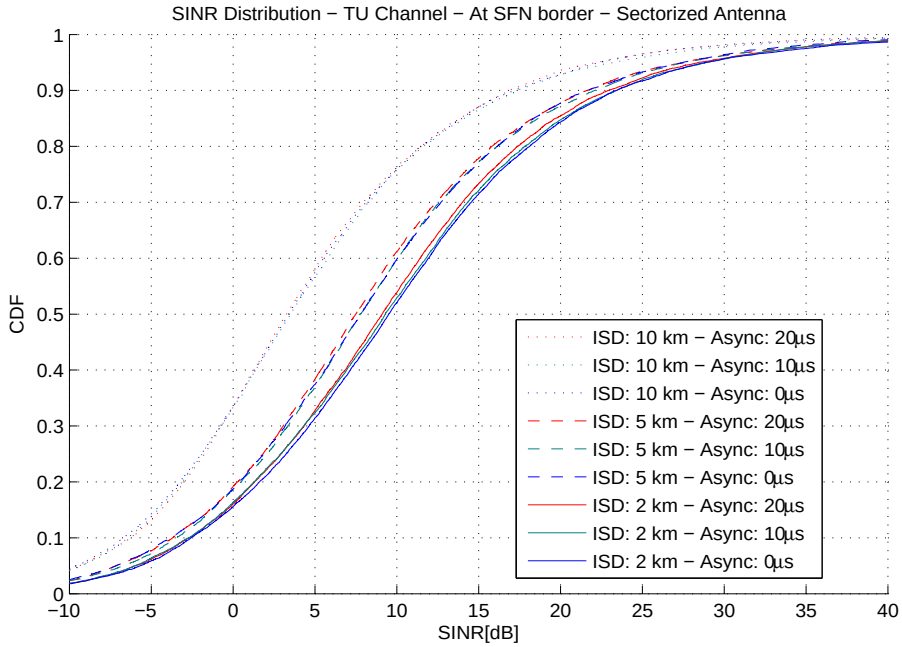

Figure 7.2: The impact of asynchronity and ISD on SINR distribution at the border of the SFN

7.1.2 Cells switched off or sending another MBMS

This paragraph studies the effect of cells inside the SFN area sending other services (unicast/MBMS) than the requested MBMS or just being switched off. On the one hand, simulations for single interfering cells compute a SINR distribution severely degraded, and on the other hand, to switch off some cell does not have a severe impact.

A simulation where 17% of the cells do not send a signal has been run. The resulting SINR is very similar of the curves in Figures 7.1 and 7.2 and thus is not given in this report. There are no notable effects on the SINR for both at the center of the network and at the border of another SFN.

On the contrary, if 17% of cells are sending an interfering signal, at the center of the network the SINR degradation is important (Figures 7.1 and 7.2). The SINR distribution is simulated in the central cell; 17% of the cells, excluding the nearest cells, are sending another service than the requested MBMS. Comparing Figure 7.1 and Figure 7.4(a) shows the degradation for the different case of ISD and asynchronity. For the small ISD, the SINR distribution is severely degraded

up to 10dB. This degradation is attenuated if the network incorporates already asynchronity. For the high ISD case, interfering cells are further and there is almost no repercussion. The same simulation can be computed at the SFN border, but as the interference level is already high, no real degradation can be noticed.

In general, for an SFN, the entire cells must send the same service to preserve the quality of the SINR among the network.

Simulation in a cell sending unicast or an other MBMS than the rest of the network shows that the performance in this type of cell are really poor (Figure 7.4(b)). Alternatively, unicast or other service transmission in a single network could be improved by introducing a guard interval of cells around the cell sending its own service. Simulations have been run by switching a tier of cells around the central cell, but the performance inside the central cell is still low (and worse in the guard interval). However, it can be noticed that the simulation is close to the performance at the border of a SFN especially for the low ISD case. For an ISD equivalent to 10 km, the SINR is more degraded because at the edge of the cell the only supporting source is very far.

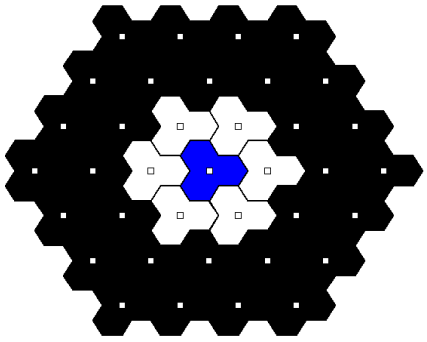

Figure 7.3: Cells guard interval concept

To conclude, allowing single cell services degrades the SINR in the overall of the network only in the low ISD case. Introducing a guard interval permits enhancing the SINR in the cell sending the unicast, but the performance is still low.

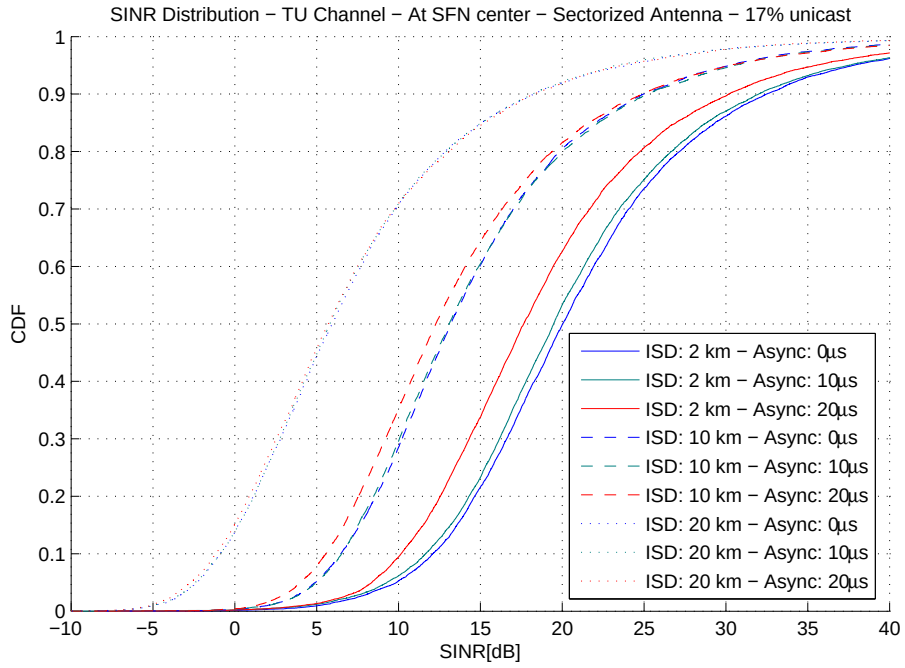

(a) SINR in the SFN where 17% of the cells (excluding the nearest cell) are sending another service than the requested MBMS

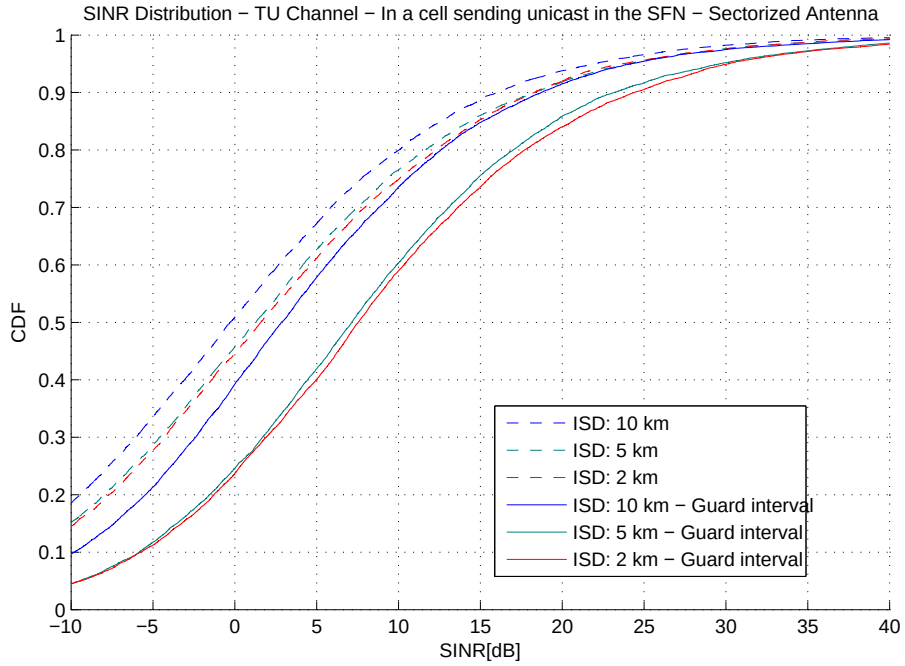

(b) In a cell sending unicast

Figure 7.4: Cell sending other service than the requested MBMS

7.2 SFN with relays

In this section, relays are now introduced in the SFN and the empirical SINR cumulative distribution is simulated. The impact of relays numbers, positions, gains and protocols are studied. Each cell is fed by fixed RSs with omnidirectional transmit antenna and a macro BS with a sectorized antenna located at the center of the cell. Most of the simulation parameters are from Table 6.4. If not specified, the simulations are run with 3 relay stations per cell applying fixed gain relaying under full-duplex protocol. The default ISD is 2 km.

7.2.1 Impact of the relay gains

In Chapter 5, the theoretical average SINR of the different relay gains has been derived for the general Nakagami fading. In this chapter, we just consider the case of Rayleigh fading which is a specific case of Nakagami fading with $m = 1$. Now recalling these results, the signal/interference amplification and noise amplification term for both fixed gain and variable gain are

$$\mathcal{E}\{|\beta^{FG}h_{SR}|^2\} = \frac{\sigma_{rn}^2 E_{SR}}{\sigma_{bs}^2 E_{SR} + N_0} \tag{7.1}$$

$$\mathcal{E}\{|\beta^{VG}h_{SR}|^2\} = \frac{\sigma_{rn}^2}{\sigma_{bs}^2}\, e^{\frac{N_0}{E_{SR}\sigma_{bs}^2}}\, \mathrm{E}_2\left(\frac{N_0}{E_{SR}\sigma_{bs}^2}\right) \tag{7.2}$$

$$\mathcal{E}\{|\beta^{FG}|^2\} = \frac{\sigma_{rn}^2}{\sigma_{bs}^2 E_{SR} + N_0} \tag{7.3}$$

$$\mathcal{E}\{|\beta^{VG}|^2\} = \frac{\sigma_{rn}^2}{E_{SR}\sigma_{bs}^2}\, e^{\frac{N_0}{E_{SR}\sigma_{bs}^2}}\, \mathrm{E}_1\left(\frac{N_0}{E_{SR}\sigma_{bs}^2}\right). \tag{7.4}$$

Interestingly for Rayleigh fading, it can be shown that the variable gain amplifies more the noise in average than the fixed gain. If we denote $x = \frac{N_0}{E_{SR}\sigma_{bs}^2}$, we can rewrite the noise amplification factor such that,

$$\mathcal{E}\{|\beta^{FG}|^2\} = \frac{\sigma_{rn}^2}{N_0}\frac{x}{1+x} \tag{7.5}$$

$$\mathcal{E}\{|\beta^{VG}|^2\} = \frac{\sigma_{rn}^2}{N_0} e^x\, \mathrm{E}_1(x)x, \tag{7.6}$$

by using [4, Eq. 5.1.19]: $\frac{1}{x+1} < e^x\, \mathrm{E}_1(x)$ for $x > 0$, the result follows that

$$\mathcal{E}\{|\beta^{FG}|^2\} < \mathcal{E}\{|\beta^{VG}|^2\} \tag{7.7}$$

It follows also from the fact that the average transmit power is constant for both fixed gain and variable gain that

$$\mathcal{E}\{|\beta^{VG} h_{SR}|^2\} < \mathcal{E}\{|\beta^{FG} h_{SR}|^2\} \tag{7.8}$$

meaning that the fixed gain amplifies more the signal and thus the interference than the variable gain. It was also proven in [14] that the fixed gain implies a higher average SNR than the variable gain.

After simulations, these different behaviors of the two gains do not seem to impact much the results. The simulation in Figure 7.5 shows that the fixed gain performed only slightly better than the variable gain for a high ISD but the difference can be considered negligible.

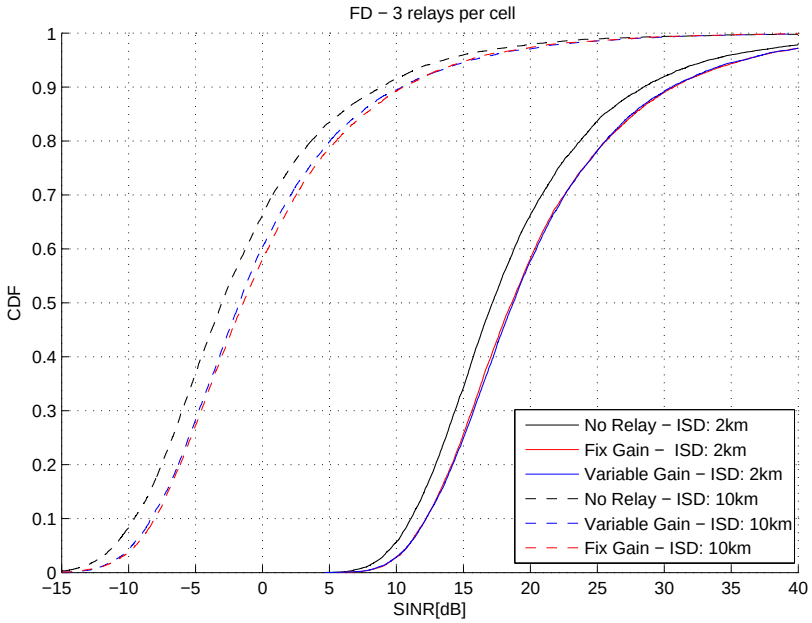

Figure 7.5: Comparision of the relay gains

7.2.2 Half-duplex versus full-duplex

Two types of transmission protocol have been presented in Chapter 5, the so-called full-duplex and half-duplex protocols[1]. Contrary to full-duplex where BSs and RSs transmit simultaneously, the half-duplex protocol shares the transmission time between the direct link and the relay link. This feature allows to apply different combing method while full-duplex does have inherent combining but uncontrolled

1. An analytical comparison of these two protocols without direct link may be found in [49].

unless feedback information may be obtained [54]. Another advantage of half-duplex is the fact that the time of reference for the demodulation is chosen separately for the two branches. Nevertheless, in order to overcome the full-duplex protocol, half-duplex should improve the SINR in a consequent amount to compensate for the loss of 1/2 in the transmission rate. Using the approximation of Equation 4.10, the capacity for one subcarrier is approximately

$$\mathcal{C}_{FD} \lessapprox \log_2(1+\Gamma_{FD}), \quad \mathcal{C}_{HD} \lessapprox \frac{1}{2}\log_2(1+\Gamma_{HD}) \tag{7.9}$$

for full-duplex and half-duplex, respectively.

If the average SINR is much greater than one, $\Gamma \gg 1$, which from the previous simulation is the case for example when the ISD is equal to 2 km, we may approximate the capacity further as follows

$$\mathcal{C}_{FD} \lessapprox \log_2(\Gamma_{FD}) \approx \frac{\ln 10}{10\ln 2}\Gamma_{FD}[\text{dB}] \tag{7.10}$$

$$\mathcal{C}_{HD} \lessapprox \frac{1}{2}\log_2(\Gamma_{HD}) \approx \frac{1}{2}\frac{\ln 10}{10\ln 2}\Gamma_{HD}[\text{dB}]. \tag{7.11}$$

So, in order to attain the same transmission rate we must have $\Gamma_{HD}[\text{dB}] = 2\Gamma_{FD}[\text{dB}]$, which means that the SINR with half-duplex should be the square of the SINR with full-duplex in a linear scale. Not surprisingly, simulations show that the half-duplex protocol does not manage to reach the performance with selection combining and equal gain combining (Figure 7.6). The gap is so important that the performance is worse than for an SFN without relays and there are few reasons to believe that applying maximum ratio combining will help.

On the other hand, if the average SINR is very close to zero, by Taylor expansion we may approximate the capacity as follows

$$\mathcal{C}_{FD} \lessapprox \log_2(1+\Gamma_{FD}) \approx \frac{1}{\ln 2}\Gamma_{FD} \tag{7.12}$$

$$\mathcal{C}_{HD} \lessapprox \frac{1}{2}\log_2(1+\Gamma_{HD}) \approx \frac{1}{2}\frac{1}{\ln 2}\Gamma_{HD}. \tag{7.13}$$

So, in order to attain the same transmission rate we must have $\Gamma_{HD}[\text{dB}] = \Gamma_{FD}[\text{dB}] + 3\text{dB}$. Unfortunately, simulations shows that half-duplex protocol does not manage to reach this gain in the context of a low SINR in a high ISD case of 10 km (Figure 7.7).

To conclude, according to our simulations, the full-duplex protocol offers largely better performance than the half-duplex protocol.

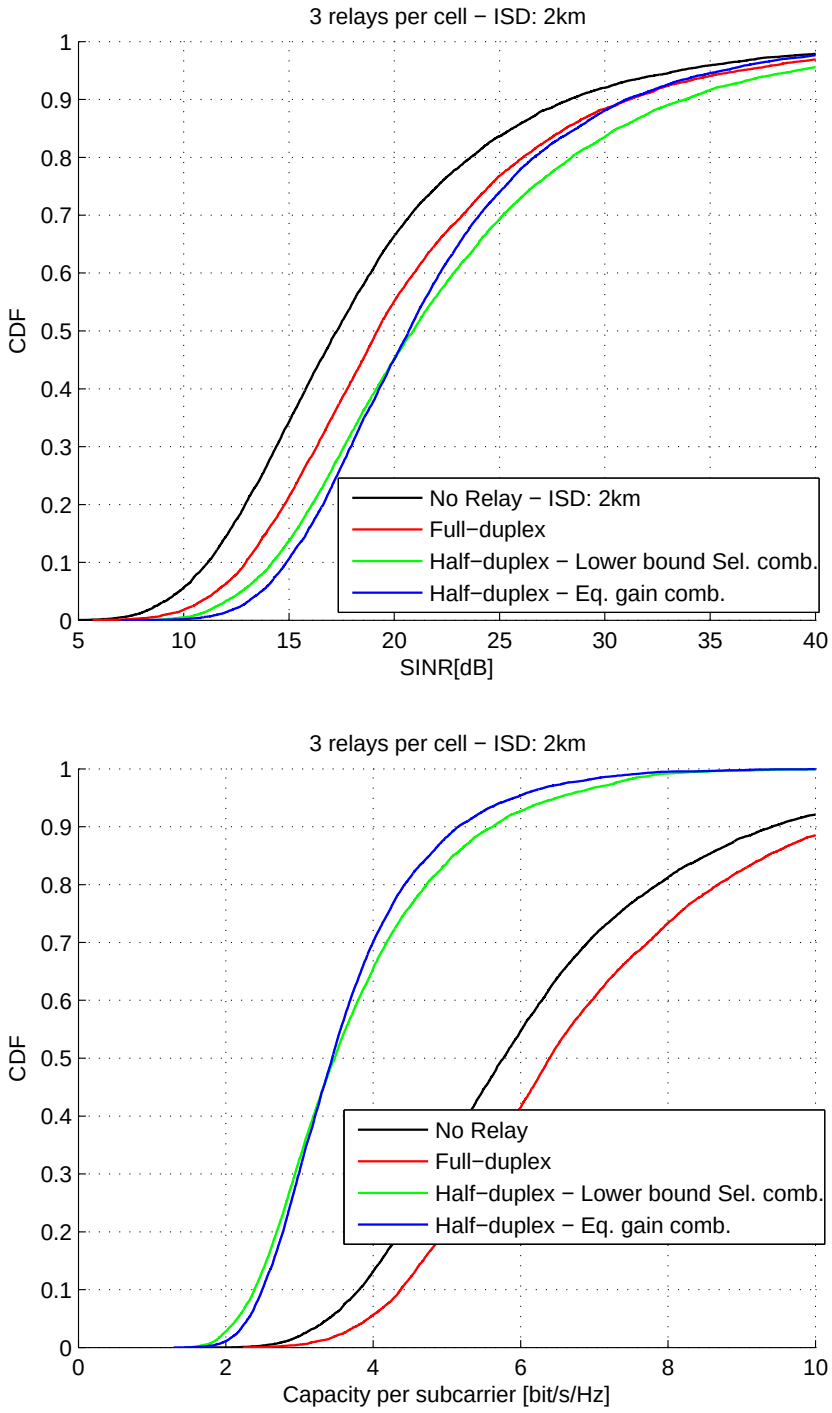

Figure 7.6: Comparison of full-duplex and half-duplex protocol - ISD: 2 km

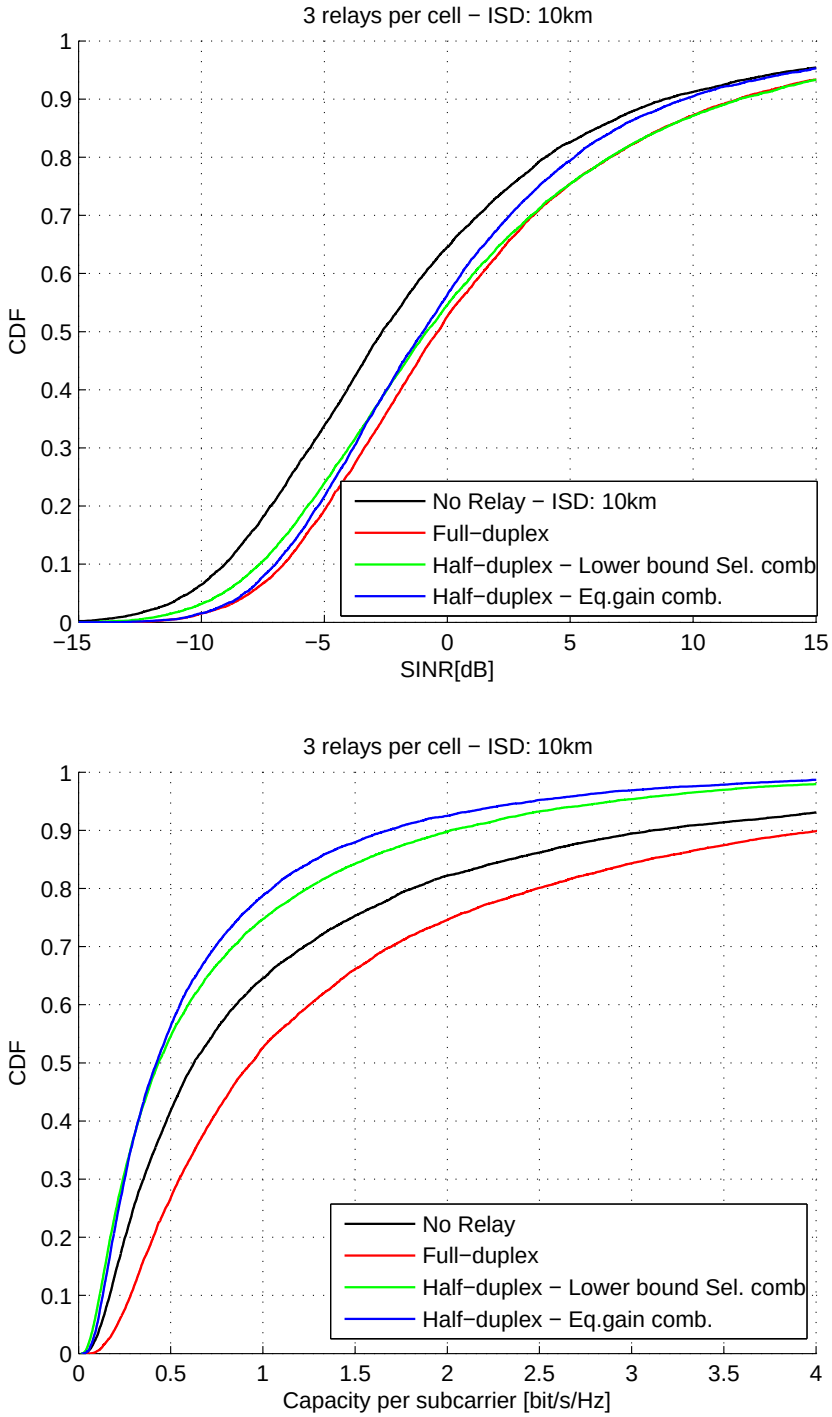

Figure 7.7: Comparison of full-duplex and half-duplex protocol - ISD: 10 km

7.2.3 Impact of relay topology

In this section, we study the impact of the number and the position of the relays. In Figure 7.8 the SINR is plotted for 3, 6, 8, 9, 12 and 15 relays per cell; also two different repartitions are used for 3 and 6 relays per cell. The different scenarios are described in Figure 7.9 where the repartition of the RSs and the BSs are drawn for the central cell and the first tier of the neighboring cells. It can be noticed that only the scenarios (a), (e) and (h) form an equidistant repartition of the access point (BSs + RSs).

The simulation shows an improvement of around 2 dB per addition of 3 relays per cell (which means 1 relay per sector) regularly from 3 to 9, 9 to 12, and 12 to 15 relays. The improvement does not seem to reduce with an increasing density of relays. Figure 7.11 plots the SINR for a fixed number of relays (six) but with different positions, it is noticed that the worst case is when the relays are closer to the BSs, the performance is then equal than with three relays per cell. After this, when the relays are located in the same area presents the next worst case scenario, and in general, an equirepartition of the access points gives a better performance. This is also why scenario (d) performs better than scenario (c) in which there is a 'gap' on the vertex of the sector. Some other figures are given in the Appendix section (Figures A.1, A.2 and A.3), they give a map of the SINR in the central cell for a different number of relays. The SINR is computed every 5m which is a slightly more than the order of the shadowing. The irregularities in the graph are due to shadowing.

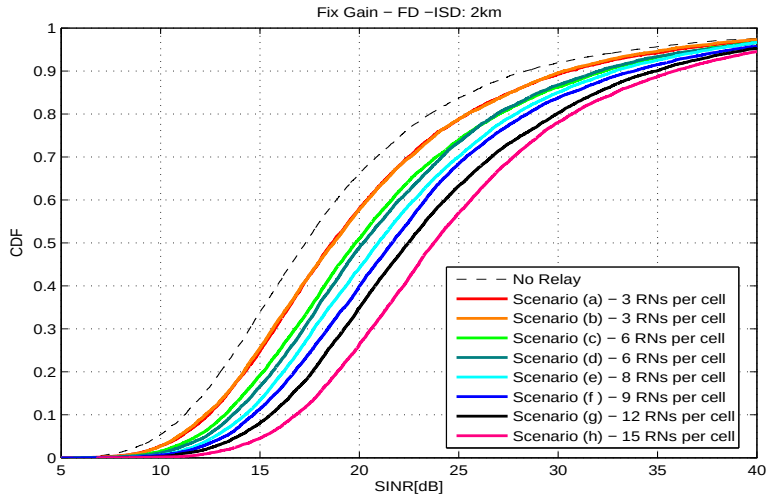

Figure 7.8: Corresponding SINR of the six different scenarios depicted in Figure 7.9

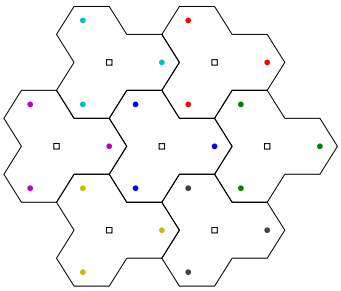

(a) 3 relays per cell

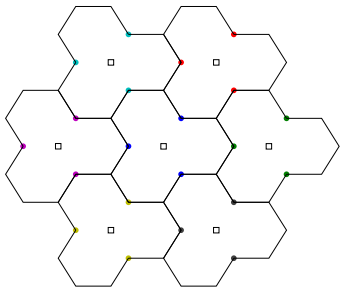

(b) 3 relays per cell

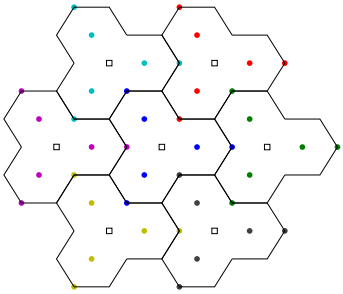

(c) 6 relays per cell

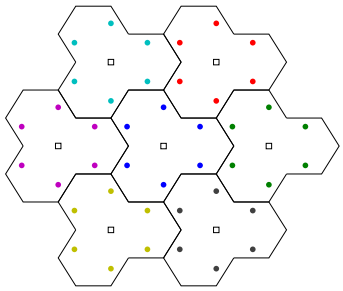

(d) 6 relays per cell

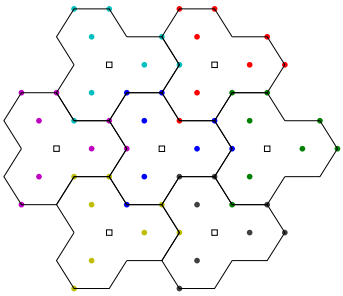

(e) 8 relays per cell

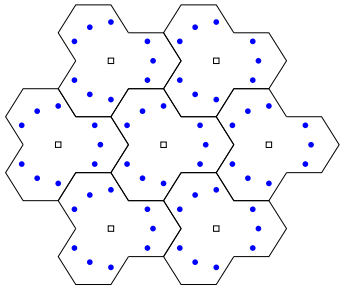

(f) 9 relays per cell

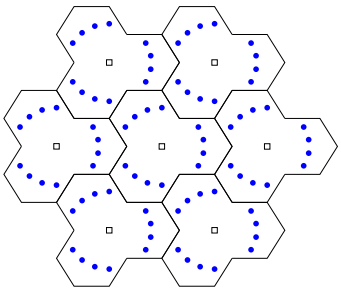

(g) 12 relays per cell

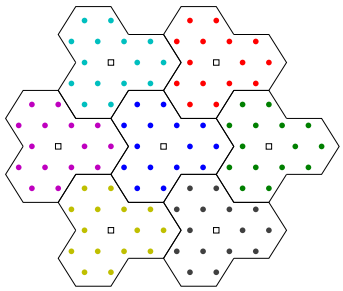

(h) 15 relays per cell

Figure 7.9: Six topology scenarios

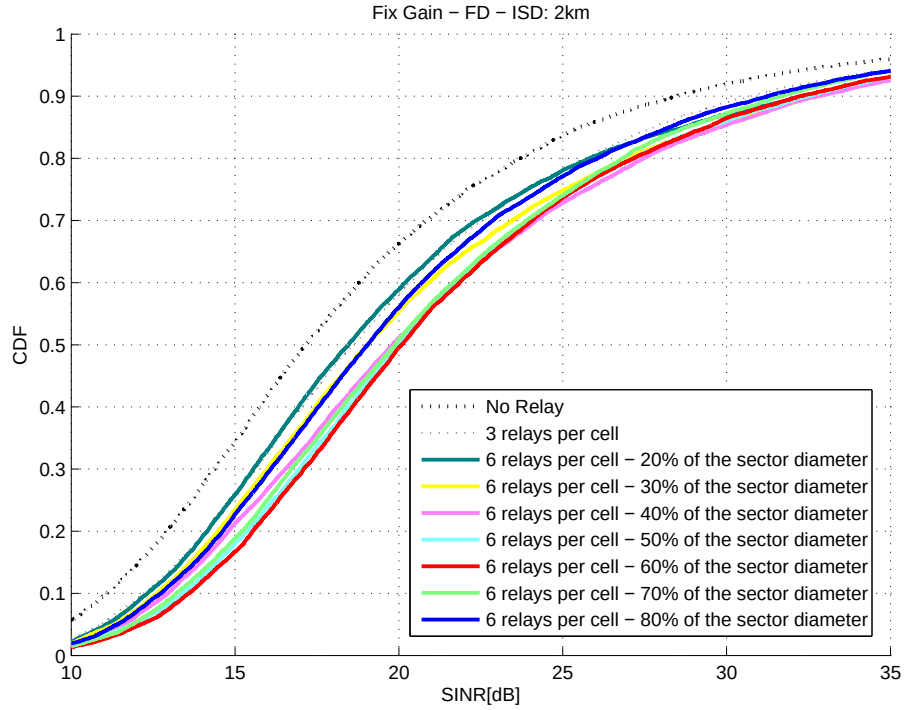

(a)

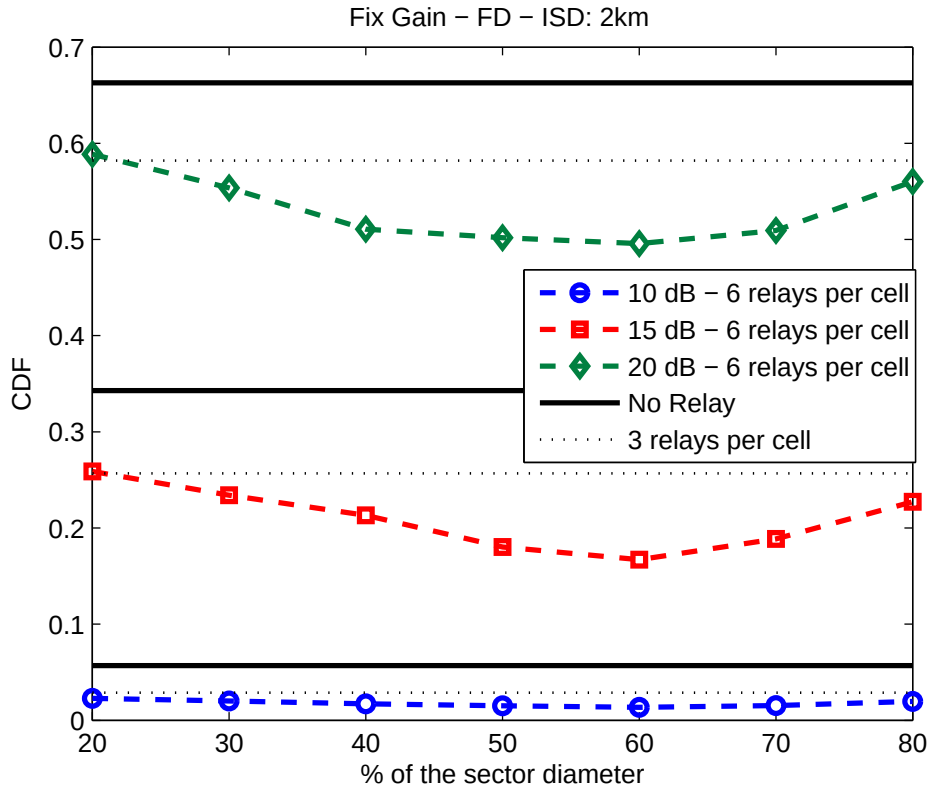

(b)

Figure 7.10: Evolution of the SINR with the relay positions

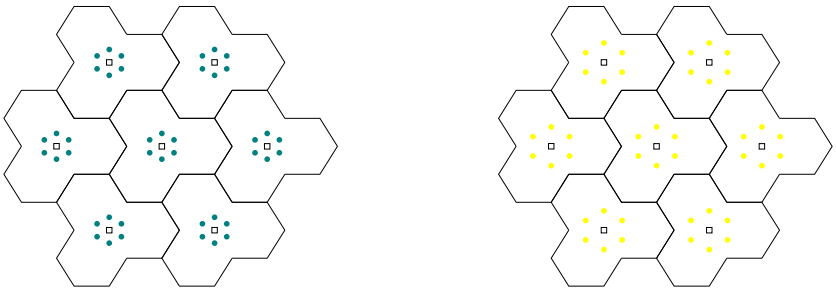

(a)

(b)

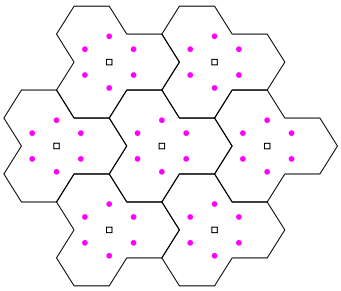

(c)

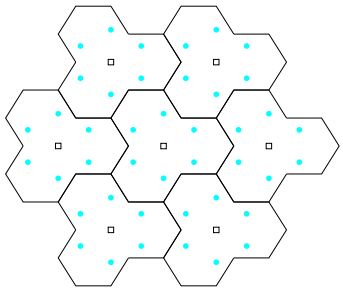

(d)

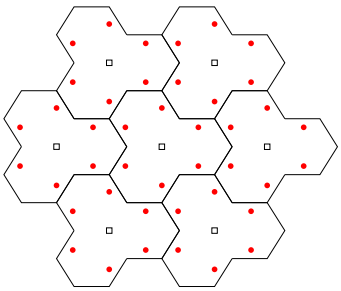

(e)

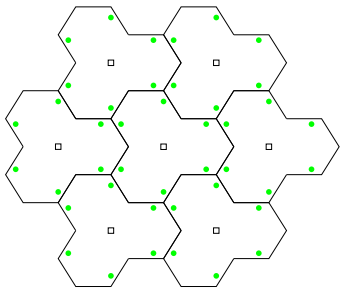

(f)

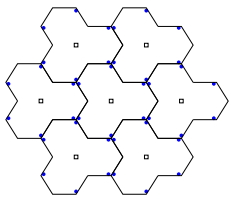

(g)

Figure 7.11: Evolution of the SINR with the relay positions

7.2.4 Performance at the SFN area borders

This last section aims to show that relaying can be used to improve the performance at the border of two SFNs. As seen previously, the performance is drastically decreased at the edge of an SFN. We have simulated the average SINR for 3, 6 and 9 relays per cell or equivalently 1, 2 and 3 relays per sectors. It appears that the performance improvement with relaying is much more important at the border of the SFN than at its center, roughly a double in decibel scale. One relay per sector adds up to 5 dB on the SINR, then the improvement for two relays per sector is less important but still significant, with three relays per sector we reach an improvement of 10 dB. However, the improvement in the performance seems to diminish with the increase of relay's number on the contrary than at the central cell. In this scenario, the addition of relays has the specific feature of decreasinf greatly the probability of a very low SINR.

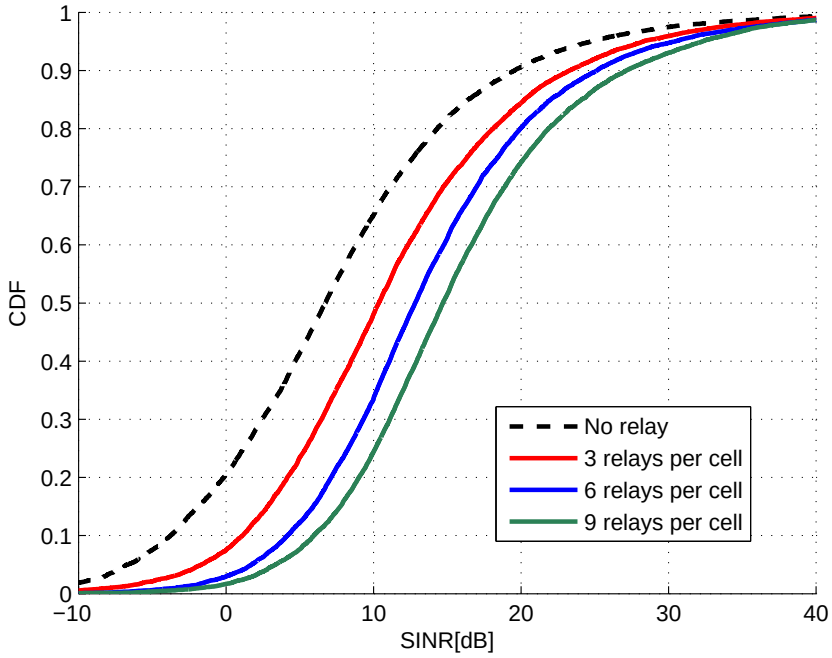

Figure 7.12: SFN with relays - area border performance

Chapter 8

Conclusions and future work

Conventionally, broadcast is considered as a drawback in wireless communication systems due to interference and requirement for frequency planning. This thesis considers the recent single-frequency relay network concept which exploits the broadcast nature of the wireless channel.

As a background, the mobile radio channel and its statistical modeling was reviewed . A summary was made of the basic principles of the widely used OFDM modulation. Some classical relaying concepts were presented with derivations of corresponding average SINRs used later in simulations.

A simulator of an OFDM-based SFN was built in order to evaluate different relaying concept in downlink broadcast communication. The simulator development was described and explained. Simulations were presented with results on the SFN area deployment aspect: impact of asyncronity in the SFN, size of the ISD, as well as introduction of unicast transmission in the SFN.

Finally, simulations of the SFN performance with fixed relay deployment are presented. The difference in behaviors of the fixed and variable gain shown theoretically appears to be negligible in the simulation. Our simulations have verified the capability of relaying to improve the system capacity and specially cell edge performance. According to our simulation, it was concluded that full-duplex protocol outperforms greatly the half-duplex protocol. The last results are concentrated in the optimization of the relays positions.

Future possible work could include a deeper mathematical analysis on the condition for correlation models among the large scale parameters to be valid; statistical analysis for the instantaneous SINR of an OFDM system and a justification by

mathematical analysis or/and simulations of the approximation of the average of the instantaneous SINR used in Chapter 4. A last suggestion would be to consider the relay self-interference.

Appendix A

SINR map

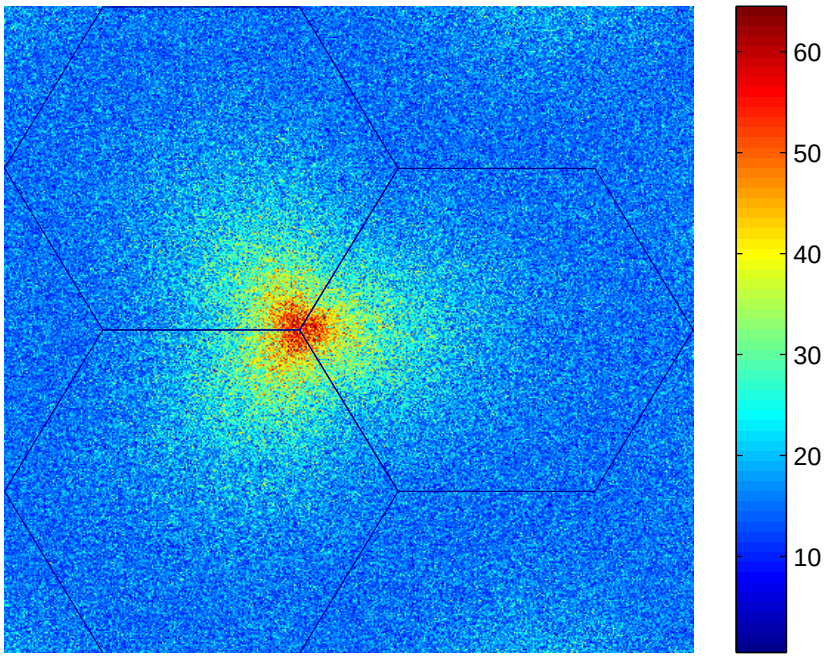

Figure A.1: Cell without relays

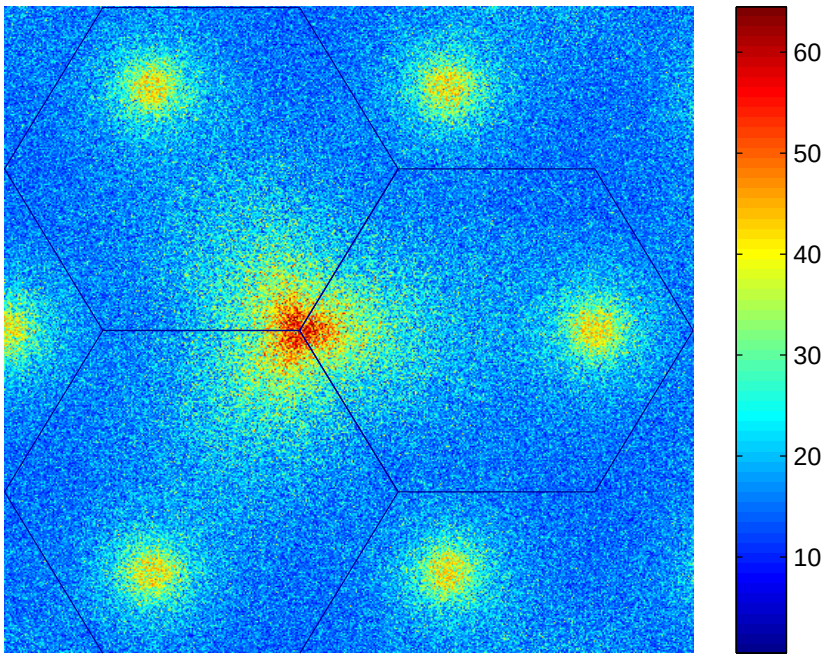

Figure A.2: Cell with 3 relays

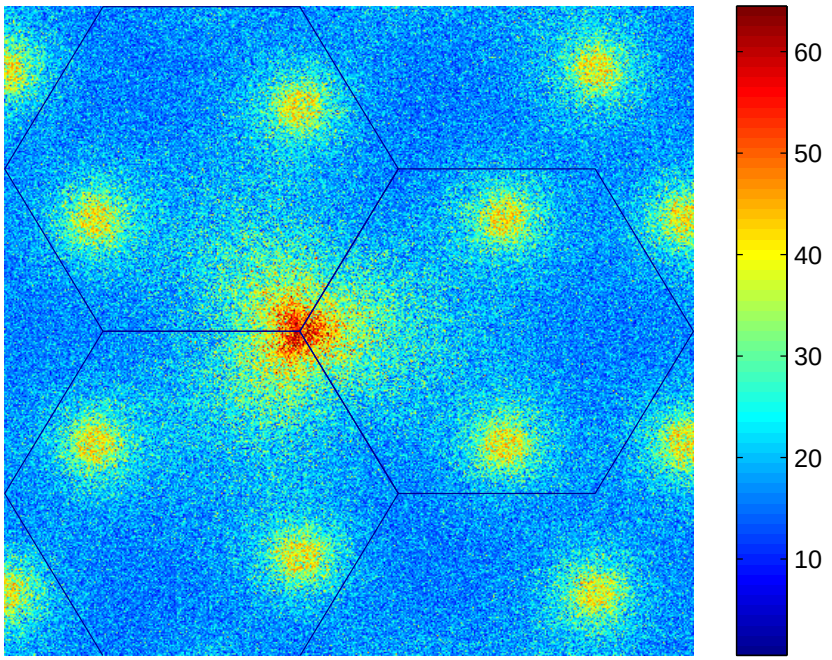

Figure A.3: Cell with 6 relays

Bibliography

[1] 3GPP. Physical layer for evolved utra. Technical Report TR 25.814, 3GPP, September 2006.

[2] WG3/WG5 TSG-C 3GPP2. 1xev-dv evaluation methodology - addendum - v6. Technical Report MSU-CSE-00-2, 3GPP2, July 2001.

[3] Bello P. A. Characterization of randomly time-variant linear channels. *IEEE Trans. Comm. Syst.*, 11:360–393, 1963.

[4] M. Abramowitz and I. A. Stegun. *Handbook of Mathematical Functions with Formulas, Graphs, and Mathematical Tables*. Dover, 1970.

[5] A. Algans, K.I. Pedersen, and P.E. Mogensen. Experimental analysis of the joint statistical properties of azimuth spread, delay spread, and shadow fading. *Selected Areas in Communications, IEEE Journal on*, 20(3):523–531, Apr 2002.

[6] H.W. Arnold, D.C. Cox, and R.R. Murray. Macroscopic diversity performance measured in the 800-mhz portable radio communications environment. *Antennas and Propagation, IEEE Transactions on*, 36(2):277–281, Feb 1988.

[7] Dan Avidor and Sayandev Mukherjee. Hidden issues in the simulation of fixed wireless systems. *Wirel. Netw.*, 7(2):187–200, 2001.

[8] M. Batariere, K. Baum, and T.P. Krauss. Cyclic prefix length analysis for 4G OFDM systems. In *Vehicular Technology Conference, 2004. VTC2004-Fall. 2004 IEEE 60th*, volume 1, pages 543–547 Vol. 1, Sept. 2004.

[9] E. Biglieri. *Coding for Wireless Channels*. Springer, 2005.

[10] G. Calcev, D. Chizhik, B. Goransson, S. Howard, H. Huang, A. Kogiantis, A.F. Molisch, A.L. Moustakas, D. Reed, and Hao Xu. A wideband spatial channel model for system-wide simulations. *Vehicular Technology, IEEE Transactions on*, 56(2):389–403, March 2007.

[11] S. Celebi. Interblock interference (ibi) and time of reference (tor) computation in OFDM systems. *Communications, IEEE Transactions on*, 49(11):1895–1900, Nov 2001.

[12] L. M. Correia. *Wireless Flexible Personalized Communications*. COST.

[13] Bernhard Walke Daniel C. Schultz. Fixed relays for cost efficient 4g network deployments: An evaluation. *The 18th Annual IEEE International Symposium on Personal, Indoor and Mobile Radio Communications (PIMRC'07)*, 2007.

[14] Xitirnin Deng and A.M. Haimovich. Power allocation for cooperative relaying in wireless networks. *Communications Letters, IEEE*, 9(11):994–996, Nov. 2005.

[15] William Feller. *An Introduction to Probability Theory and Its Applications*. Wiley, 1968.

[16] R. G. Gallager. *Information Theory and Reliable Communication*. New York: Wiley, 1968.

[17] D. Giancristofaro. Correlation model for shadow fading in mobile radio channels. *Electron. Lett.*, 32:958–959, May 1996.

[18] N. Gogate, D. Avidor, and S.S. Panwar. Simulation study of a fixed wireless access system. *Universal Personal Communications, 1998. ICUPC '98. IEEE 1998 International Conference on*, 1:209–215 vol.1, Oct 1998.

[19] Andrea J. Goldsmith. *Design and Performance of High-Speed Communication Systems over Time-Varying Radio Channels*. PhD thesis, EECS Department, University of California, Berkeley, 1994.

[20] V. Graziano. Propagation correlations at 900 mhz. *IEEE Transactions on Vehicular Technology*, VT-27, 1978.

[21] F. Graziosi, M. Pratesi, M. Ruggieri, and F. Santucci. A multicell model of handover initiation in mobile cellular networks. *Vehicular Technology, IEEE Transactions on*, 48(3):802–814, May 1999.

[22] F. Graziosi and F. Santucci. A general correlation model for shadow fading in mobile radio systems. *Communications Letters, IEEE*, 6(3):102–104, Mar 2002.

[23] 3GPP/3GPP2 SCM Ad-Hoc Group. Spatial channel model text description. *v3.3*, March 2003.

[24] M. Gudmundson. Correlation model for shadow fading in mobile radiosystems. *Electron. Lett.*, 27:2145–2146, Nov. 1991.

[25] M.A. Haleem, D. Avidor, and R. Valenzuela. Fixed wireless access system with autonomous resource assignment. *Personal, Indoor and Mobile Radio Communications, 1998. The Ninth IEEE International Symposium on*, 3:1438–1442 vol.3, Sep 1998.

[26] M.O. Hasna and M.-S. Alouini. A performance study of dual-hop transmissions with fixed gain relays. *Wireless Communications, IEEE Transactions on*, 3(6):1963–1968, Nov. 2004.

[27] M. Hata. Empirical formula for propagation loss in land mobile radio services. *IEEE Transactions on Vehicular Technology*, 29, 1980.

[28] L. Vuokko J. Salo and P. Vainikainen. Why is shadow fading lognormal? *Proc. International Symposium on Wireless Personal Multimedia Communications Aalborg, Denmark*, pages 522–526, 2005.

[29] S.K. Wilson P.O. Börjesson J.J. van de Beek, P. Ödling. Orthogonal frequency-division multiplexing (OFDM). *the International Union of Radio Science (URSI)*, 2002.

[30] J.Walfisch and H.L. Bertoni. A theoretical model of uhf propagation in urban environments. *IEEE Trans. Antennas Propagat.*, 36, 1988.

[31] Hoon Kim and Youngnam Han. Enhanced correlated shadowing generation in channel simulation. *Communications Letters, IEEE*, 6(7):279–281, Jul 2002.

[32] T. Klingenbrunn and P. Mogensen. Modelling cross-correlated shadowing in network simulations. *Vehicular Technology Conference, 1999. VTC 1999 - Fall. IEEE VTS 50th*, 3:1407–1411 vol.3, 1999.

[33] Yu Shuan Yeh Larry J. Greenstein, Vinko Erceg and Martin V. Clark. A new path-gain/delay-spread propagation model for digital cellular channels. *IEEE Transactions on Vehicular Technology*, VOL.46, MAY 1997.

[34] Ki-Ho Lee and Dong-Ho Cho. Hierarchical constellation based adaptive relay scheme in multi-hop networks. *Communications Letters, IEEE*, 11(3):225–227, March 2007.

[35] M.J. Marsan, G.C. Hess, and S.S. Gilbert. Shadowing variability in an urban land mobile environment at 900 mhz. *Electronics Letters*, 26(10):646–648, May 1990.

[36] A. Mawira. Models for the spatial correlation functions of the (log)- normal component of the variability of vhfrthf field strength in urban environment. *PIMRC Proceedings*, pages 436–440, Boston 1992.

[37] A. Mawira. Models for the spatial correlation functions of the (log)-normal component of the variability of vhf/uhf field strength in urban environment. *Personal, Indoor and Mobile Radio Communications, 1992. Proceedings, PIMRC '92., Third IEEE International Symposium on*, pages 436–440, Oct 1992.

[38] Aris Moustakas and Achilles Kogiantis. Lognormal correlations between shadowing, delay-spread and angle-spread and for different base-stations: A unified approach. *Lucent Technologies, SCM-125-LUC-LognormalCorrelations*, July 2001.

[39] S. Mukherjee and D. Avidor. Dynamics of path losses between a mobile terminal and multiple base stations in a cellular environment. *Vehicular Technology, IEEE Transactions on*, 50(6):1590–1603, Nov 2001.

[40] S. Mukherjee and D. Avidor. Effect of microdiversity and correlated macrodiversity on outages in a cellular system. *Wireless Communications, IEEE Transactions on*, 2(1):50–58, Jan. 2003.

[41] Van Duc Nguyen and H.-P. Kuchenbecker. Intercarrier and intersymbol interference analysis of OFDM systems on time-invariant channels. In *Personal, Indoor and Mobile Radio Communications, 2002. The 13th IEEE International Symposium on*, volume 4, pages 1482–1487 vol.4, Sept. 2002.

[42] Björn Ottersten Niklas Jalden, Per Zetterberg and Laura Garcia. Inter and intra-site correlation of large scale parameters from macro cellular measurements at 1800mhz. *EURASIP Journal on Wireless Communications and Networking*, August 2007.

[43] Nokia. SFN area deployement aspect. *3GPP TSG-RAN WG3 Meeting 53 bis*, October 2006.

[44] A. Nosratinia, T.E. Hunter, and A. Hedayat. Cooperative communication in wireless networks. *Communications Magazine, IEEE*, 42(10):74–80, Oct. 2004.

[45] Minoru Okada and Shozo Komaki. Pre-dft combining space diversity assisted cOFDM. *IEEE Transactions on Vehicular Technology, VOL. 50, NO. 2, March 2001.*

[46] E. Perahia, D.C. Cox, and S. Ho. Shadow fading cross correlation between basestations. *Vehicular Technology Conference, 2001. VTC 2001 Spring. IEEE VTS 53rd*, 1:313–317 vol.1, 2001.

[47] J.G Proakis. *Digital Communications*. New York:McGraw-Hill, 1989.

[48] Bernhard H. Walke Ralf Pabst, Sayandev Mukherjee Daniel C. Schultz, Patrick Herhold; Halim Yanikomeroglu, Matthias Lott Harish Viswanathan, Wolfgang Zirwas; Mischa Dohler, and David D. Falconer; Gerhard P. Fettweis Hamid Aghvami. Relay-based deployment concepts for wireless and mobile broadband radio. *IEEE Communications Magazine*, September 2004.

[49] T. Riihonen, S. Werner, and R. Wichman. Comparison of full-duplex and half-duplex modes with a fixed amplify-and-forward relay. In *Wireless Communications and Networking Conference, 2009. WCNC 2009. IEEE*, pages 1–5, April 2009.

[50] T. Riihonen, S. Werner, and R. Wichman. Optimized gain control for single-frequency relaying with loop interference. *Wireless Communications, IEEE Transactions on*, 8(6):2801–2806, June 2009.

[51] T. Riihonen, S. Werner, R. Wichman, and J. Hamalainen. Outage probabilities in infrastructure-based single-frequency relay links. In *Wireless Communications and Networking Conference, 2009. WCNC 2009. IEEE*, pages 1–6, April 2009.

[52] T. Riihonen and R. Wichman. Power allocation for a single-frequency fixed-gain relay network. In *Personal, Indoor and Mobile Radio Communications, 2007. PIMRC 2007. IEEE 18th International Symposium on*, pages 1–5, Sept. 2007.

[53] T. Riihonen, R. Wichman, and J. Hamalainen. Diversity analysis of a parallel amplify and forward relay network. In *Signal Processing Advances in Wireless Communications, 2007. SPAWC 2007. IEEE 8th Workshop on*, pages 1–5, June 2007.

[54] T. Riihonen, R. Wichman, and J. Hamalainen. Co-phasing full-duplex relay link with non-ideal feedback information. In *Wireless Communication Systems. 2008. ISWCS '08. IEEE International Symposium on*, pages 263–267, Oct. 2008.

[55] J. Salo, L. Vuokko, H. M. El-Sallabi, and P. Vainikainen. An additive model as a physical basis for shadow fading. *Vehicular Technology, IEEE Transactions on*, 56(1):13–26, Jan. 2007.

[56] S. R. Saunders. *Antennas and Propagation for Wireless Communication. Systems*. New York: Wiley, 1999.

[57] T.B. Sorensen. Correlation model for slow fading in a small urban macro cell. In *Personal, Indoor and Mobile Radio Communications, 1998. The Ninth IEEE International Symposium on*, volume 3, pages 1161–1165 vol.3, Sep 1998.

[58] T.B. Sorensen. Slow fading cross-correlation against azimuth separation of base stations. *Electronics Letters*, 35(2):127–129, Jan 1999.

[59] H. Steendam and M. Moeneclaey. Analysis and optimization of the performance of OFDM on frequency-selective time-selective fading channels. *Communications, IEEE Transactions on*, 47(12):1811–1819, Dec 1999.

[60] Bogdan Timus. Cost analysis issues in a wireless multihop architecture with fixed relays. *Vehicular Technology Conference. Spring 2005 IEEE 61st.*

[61] J. van Rees. Cochannel measurements for interference limited small cell planning. *Int. J. Electron. Commun.*, 41(5):318–320, 1987.

[62] A. J. Viterbi. *CDMA: Principles of Spread Spectrum Communication.* MA: Addison-Wesley, 1995.

[63] A.J. Viterbi, A.M. Viterbi, K.S. Gilhousen, and E. Zehavi. Soft handoff extends cdma cell coverage and increases reverse link capacity. *Selected Areas in Communications, IEEE Journal on*, 12(8):1281–1288, Oct 1994.

[64] R. Wang, D.C. Cox, H. Viswanathan, and S. Mukherjee. A first step toward distributed scheduling policies in cellular ad hoc networks. In *Mobile and Wireless Communications Network, 2002. 4th International Workshop on*, pages 8–12, 2002.

[65] J. Weitzen and T.J. Lowe. Measurement of angular and distance correlation properties of log-normal shadowing at 1900 mhz and its application to design of pcs systems. *Vehicular Technology, IEEE Transactions on*, 51(2):265–273, Mar 2002.

[66] T. Kawano Y. Okumura, E. Ohmori and K. Fukada. Field strength and its variability in vhf and uhf land-mobile radio service. *Review of the Electrical Communication Laboratory*, 16, 1968.

[67] K. Yamamoto, A. Kusuda, and S. Yoshida. Impact of shadowing correlation on coverage of multihop cellular systems. In *Communications, 2006. ICC '06. IEEE International Conference on*, volume 10, pages 4538–4542, June 2006.

[68] X. Yang, S. Ghaheri-Niri, and R. Tafazolli. Downlink soft handover gain in cdma cellular network with cross-correlated shadowing. *Vehicular Technology Conference, 2001. VTC 2001 Fall. IEEE VTS 54th*, 1:276–280 vol.1, 2001.

[69] K. Zayana and B. Guisnet. Measurements and modelisation of shadowing cross-correlations between two base-stations. *Universal Personal Communications, 1998. ICUPC '98. IEEE 1998 International Conference on*, 1:101–105 vol.1, Oct 1998.

[70] Jingiun Zhang and V.A. Aalo. Effect of branch correlation on a macrodiversity system in a shadowed rician fading channel. *Electronics Letters*, 34(1):18–20, Jan 1998.